MARCH 1990

FOM-INSTITUUT
VOOR
PLASMAFYSICA
RIJNHUIZEN

ASSOCIATIE
EURATOM-FOM

HIGH-BETA STABILITY STUDIES OF JET DISCHARGES WITH THE NUMERICAL PROGRAM HBT

G.T.A. HUYSMANS, R.M.O. GALVÃO*, AND J.P. GOEDBLOED

FOM-INSTITUUT VOOR PLASMAFYSICA RIJNHUIZEN, NIEUWEGEIN, THE NETHERLANDS
*INSTITUTO DE PESQUISAS ESPACIAIS, SÃO JOSÉ DOS CAMPOS, BRAZIL

RIJNHUIZEN REPORT 90-193

REPORT ON JET CONTRACT
NO. JT9/9003 PART I

PROJECT LEADER: J.P. GOEDBLOED

This work was performed as part of the research programme of the association agreement of Euratom and the 'Stichting voor Fundamenteel Onderzoek der Materie' (FOM) with financial support from the 'Nederlandse Organisatie voor Wetenschappelijk Onderzoek' (NWO) and Euratom.

POSTBUS 1207
3430 BE NIEUWEGEIN
NEDERLAND
EDISONBAAN 14
3439 MN NIEUWEGEIN
TEL. 03402 - 31224
TELEFAX 03402 -31204
TELEX 47380 RIJNHZ NL

CONTENTS page

ABSTRACT v

I. INTRODUCTION 1

II. STABILITY AT HIGH BETA 2

III. BALLOONING STABILITY OF JET HIGH BETA DISCHARGES 5

A. Broad pressure profiles (discharge #19970) 5

B. Peaked pressure profiles (discharges #20272 and #20302) 7

C. Conclusions 10

IV. STABILITY OF SINGLE AND DOUBLE X-POINT PLASMAS 12

A. Stability of up-down asymmetric equilibria 12

B. Influence of the change from double to single X-point 13

V. EXTERNAL KINK MODES 15

A. Global kink modes 15

B. Peeling modes 15

REFERENCES 19

FIGURES 22

ABSTRACT

This report describes the analysis of the MHD properties of JET discharges with the stability code HBT and its recently developed up-down asymmetric version HBTAS.

The ballooning stability properties of the latest (July 1989) high-beta discharges produced at JET have been analyzed with HBT. One example of a discharge with a broad pressure profile is shown to be close to the ballooning stability limit in the region of the largest pressure gradient. The equilibrium that is marginally stable, with the same q-profile, shows that this limit is approached only locally but that much higher beta values are possible if the region of the large gradients can be increased towards the edge of the plasma. The evaluated high-beta discharges with a peaked pressure profile, produced with or without the injection of a pellet, are shown to exceed the ballooning limit in the plasma center by a factor of 1.5 to 2 if a monotonic q-profile is assumed. The stabilizing influence of raising q on axis is shown to be too small to stabilize this instability. Complete stabilization can be obtained with a non-monotonic q-profile with relatively large negative shear in the plasma center.

The code HBTAS has been exploited to investigate the influence on the ballooning stability of a change from double to single X-point plasma cross-sections, as used in some of the high-β discharges in JET. The effects on the stability turn out to be relatively small for the shapes considered.

Both global external kink modes and edge localized peeling modes have been investigated in the high-β ordering. Beta limits, in agreement with the Troyon scaling, are found for the global modes whereas the peeling modes turned out to become stable when the elongation of the plasma cross-section was increased from circular to elongated.

I. INTRODUCTION

The latest high-beta discharges (July, October 1989) produced at JET [1] have reached values of β close to the maximum attainable one with respect to MHD stability as predicted by the Troyon limit (see Fig. 1). Here $\beta_{Troyon} = 2.8\ I[MA] / B_0[T]\ a[m]$. The highest beta obtained is about 100% of the Troyon limit. These high-beta values were reached in a double-null X-point configuration during the H-mode phase. A low toroidal field (1.2 - 1.5 T) was used in order to take advantage of the scaling of the confinement time with the toroidal field of JET H-mode plasmas [2]: $\tau_E \sim I_p^{2/3} B_0^{1/3} P^{-1/2}$ and $\beta/\beta_{Troyon} \sim \tau_E/B_0$. The additional heating was provided by up to 15 MW of neutral beam injection power and around 5 MW of ICRH. The high beta discharges were produced in the carbon tiled JET vessel coated with a monolayer of Beryllium.

In this report we will analyze the MHD stability properties of JET discharges by directly inserting measured experimental profiles into the MHD stability code HBT (≡ High Beta Tokamak), developed at the FOM-Instituut voor Plasmafysica by J.P. Goedbloed and coworkers [3 - 7]. The details about the interfacing of the diagnostic data with the stability code and a complete documentation of HBT, and of the up-down asymmetric version HBTAS, are to be found in the accompanying report "Documentation of the high-beta stability codes HBT and HBTAS" [8]. All the technical details on the calculations are described there. Here, we will keep the physics to the foreground.

The organization of this report is as follows. In Sec. II some introductory notions of tokamak stability at high β are discussed. The main effort, concerned with the stability of ballooning modes in JET, is described in Sec. III. Here, we extensively describe the analysis of experimental JET discharges with the code HBT. Section IV contains the first results of the analysis of up-down asymmetric plasmas, like single X-point high-β or divertor plasmas, with the new code HBTAS. Finally, Sec. V contains some results on external kink modes at high-β, using the high-beta tokamak ordering.

II. STABILITY AT HIGH BETA

Two scaling laws for stability of tokamaks at high β exist which both express the limiting beta as a function of the total plasma current. These limits broadly refer to global kink modes and local ballooning modes, respectively. For simplicity, we will refer to the first criterion as the Troyon limit for kink modes [9,10] and to the second one as the Sykes - Wesson limit for ballooning modes [11,12]. It is true that in Refs. [9,10] the whole issue of MHD stability in tokamaks at high beta was considered, but the original result was a stress on the onset of global n = 1 kink modes as being the limiting factor for beta. Similarly, Refs. [11,12] were mainly concerned with ballooning modes limiting tokamak operation at high beta. Clearly, both classes of modes have to be considered simultaneously. It is still a surprising, and unexplained, fact that both types of modes would result in a linear relationship between the optimum beta and the plasma current. This relationship may be written as:

$$<\beta>\,[\%] = g\,\frac{I_p\,[\mathrm{MA}]}{a\,[\mathrm{m}]\;B_0\,[\mathrm{T}]}\ . \tag{2.1}$$

In this form, the value of the factor g is the single number to be computed and tested against experimental data. It is another surprise that the maximum value of this factor for kink modes and for ballooning modes would be so close as they are found to be in numerical investigations. Experimentally, there is ample evidence for a limiting value of <β>, but there is no conclusive evidence for either kink or ballooning modes. In Sec. III we will show that the limiting theoretical value for ballooning modes has been reached in JET and even surpassed in limited regions of the plasma, in particular at the magnetic axis. This is a first indication that ballooning modes might not represent the ultimate limit for β in tokamaks.

The relationship (2.1) may be cast in a form which is more appropriate for the purpose of theoretical investigation of the scaling laws. Expressing <β> in decimal form (as opposed to percentages) and I_p in amperes, one obtains an expression in usual MKSA units:

$$<\beta>/\varepsilon = f\,\frac{\mu_0 R_0 I_p}{2\pi a^2 B_0}\ , \tag{2.2}$$

where f is related to g by a simple factor:

$$f \equiv (2\pi\times 10^{-6}\times 10^{-2}/\mu_0)\,g = g/20\ . \tag{2.3}$$

Hence, $g_{\mathrm{Troyon}} = 2.8$ will correspond to $f_{\mathrm{Troyon}} = 0.14$. Next, we introduce a kind of equivalent safety factor, based on the total current [13]:

$$q^* \equiv \frac{a\,L\,B_0}{\mu_0 R_0 I_p}. \tag{2.4}$$

In terms of this quantity the Troyon - Sykes - Wesson scaling law will read

$$<\beta>/\varepsilon = f.\frac{e}{q^*}, \tag{2.5}$$

where $e \equiv L/2\pi a$ is the elongation of the plasma cross-section.

In Ref. [13] the parameter q^* was introduced for the specific purpose of studying global kink modes in toroidal geometry at high beta. It was argued that the safety factor q itself could not properly serve for that purpose since it blows up when a separatrix moves onto the plasma boundary, whereas kink stability does not appear to be very much influenced by this fact. This idea found general acceptance, as is evident by the widespread use of similar parameters measuring the current, like the "cylindrical q" parameter used in the INTOR and ITER studies:

$$q_J \equiv \frac{\pi(a^2+b^2)B_0}{\mu_0 R_0 I_p} = \frac{1}{2e}(1+b^2/a^2)\,q^*. \tag{2.6}$$

Here, we will stick to the use of q^* as defined in Eq. (2.4) since it does not depend on a particular assumption on the geometry of the plasma cross-section (Eq. (2.6) assumes elliptical geometry to define a and b).

From the definitions of $<\beta>$ and β_p,

$$<\beta> \equiv \frac{2\mu_0<p>}{B_0^2}, \qquad \text{and} \qquad \beta_p \equiv \frac{8\pi S<p>}{\mu_0 I_p^2}, \tag{2.7}$$

and the definition (2.4) for q^* one obtains a simple and exact relationship between the three parameters $<\beta>$, β_p, and q^* :

$$<\beta>/\varepsilon = \eta^{-1}\,\frac{\varepsilon\beta_p}{q^{*2}}, \tag{2.8}$$

where $\eta \equiv S/(\pi a^2 e^2)$ is a geometrical factor measuring the deviation of the plasma cross-section from a circular one. [For a circle, the area $S=2\pi a^2$ and the elongation e=1.] The importance of the relationship (2.8) is that, at high β, the overall equilibrium features are determined by the value of $\varepsilon\beta_p$, whereas global kink stability is mainly determined by the value of q^*.

How does the quadratic relationship between $<\beta>$ and q^* of Eq.(2.8) relate to the linear one expressed by Eq. (2.5)? Since kink mode stability at high β depends on both the value of $\varepsilon\beta_p$ and on q^* there is no a priori way to determine what the outcome of an optimalization study will be. Numerics tells us that a linear scaling results. The situation is different for ballooning modes. For a particular model equilibrium with a circular cross-section, it was shown by Wesson and Sykes [12] that the maximum β for ballooning modes can be written as

$$<\beta>/\varepsilon = \frac{c}{q_1^2}\,(\sqrt{q_1/q_0} - 1), \tag{2.9}$$

where it should be noticed that $q_1 = q^*$ in this case. Here, the factor $\sqrt{q_1/q_0}$ really enters as a kind of profile effect which optimizes the shear at the plasma edge. Prescribing the value of q_0, the relationship (2.9) then results in an approximately linear dependence of $<\beta>$ on $1/q^*$, at least when $q^* > 2$. Clearly, in order to get the linear scaling law, an additional ingredient is infused in the theory, viz. that $q_0 > 1$.

Since the limitation $q_0 > 1$ no longer appears to be a hard condition in tokamak operation [14], the optimization of $<\beta>$ with respect to ballooning modes should be reconsidered. It is obvious from Eq. (2.9) that there is no limit on $<\beta>$ for ballooning modes if one would be able to freely cross the $q_0 = 1$ boundary. The rationale to allow this should come from experimental evidence, but could be underpinned theoretically by the observation that, at high β, the ballooning equation only depends on the equilibrium value of the parameter $\varepsilon\beta_p$, and not on the values of q^*, q_0, or q_1. The higher order effects, giving rise to dependence on q_0 and the Mercier criterion, correspond to smaller growth rates of the modes, which can be eliminated theoretically by the use of the σ-stability concept [15]. Hence, ultimately, one should expect fast growing ballooning modes at high β to give rise to the quadratic scaling with the current as expressed by Eq. (2.8). One could express this in agreement with Eq. (2.9) by writing

$$<\beta>/\varepsilon = \frac{c}{q^{*2}} \cdot f(q_1/q_0)\,, \tag{2.10}$$

where $f(q_1/q_0)$ represents the influence of the equilibrium profiles, which is expressed solely by the factor $\varepsilon\beta_p$ in the high-β ordering.

In Fig. 2 we show an example of optimizing β with respect to ballooning modes in a circular cross-section plasma by the usual procedure of fixing $\varepsilon\beta_p$ and increasing q^* until the stability limit is reached, while either imposing the condition $q_0 > 1$ (lower curves) or dropping it (upper curves). It is evident that the ballooning stability limit is substantially increased in this manner.

If the ultimate result of pushing the current in tokamaks would be a quadratic scaling for ballooning modes and a quadratic one for kink modes, one should experimentally observe that kink modes take over at large currents. In the next section we present evidence that JET discharges have indeed crossed the theoretical ballooning limit at high β operation without dramatic loss of confinement. In order to avoid misunderstanding: we have not exploited any of the cut-off procedures discussed above. All our results are obtained on the basis of the exact ballooning equation, observing the Mercier criterion.

III. BALLOONING STABILITY OF JET HIGH BETA DISCHARGES

In this section we will concentrate on the ideal MHD stability properties of symmetric high beta discharges at JET, especially on ballooning mode stability. The high-β discharges that will be discussed below can be divided into two categories. The first consists of discharges with a broad pressure profile with large gradients near the edge of the plasma, resembling the 'classical' H-mode pressure profile. The pressure profile of the second category has a markedly triangular shape with a constant pressure gradient over most of the minor radius. Examples of both types of discharges will be discussed with respect to their ballooning stability properties. Starting from the experimental equilibrium profiles, the pressure profile that is marginally stable to ballooning modes will be calculated, keeping the q-profile constant. This will give an indication of how close the discharge is to the stability limit. This will also give the maximum achievable beta in the case that ballooning modes pose the strongest limit on the maximum beta. In section III A a discharge with a broad pressure profile will be discussed. Two discharges with peaked pressure profiles, without and with injection of a pellet respectively, are presented in sections III B1 and III B2. Conclusions are drawn in section III C.

A. BROAD PRESSURE PROFILES. (DISCHARGE #19970)

The high-beta discharges with broad pressure profiles have been produced during a sqan in low q_{cyl} values to determine whether there is any degradation of confinement with decreasing q_{cyl} [16] as was observed in DIII-D [17]. One example of this series is discharge #19970 which reached the highest beta of 3.3% which is at 65% of the Troyon limit (B_0 = 1.54T, I = 3.1 MA, a = 1.10 m, β_P = 0.43). The traces of the toroidal beta and the total input power are shown in Fig. 3. The discharge ends at 49.2 s with a disruption caused by the influx of carbon impurities. Up to the disruption there is no degradation of confinement associated with MHD activity. The MHD activity (see Fig. 4) shows an increase of the n = 3 component relative to the lower mode numbers starting at $\beta \sim 0.5\ \beta_{Troyon}$. There are no ELMs during the H-mode.

The equilibrium needed for the stability analysis was calculated with the IDENTC code [18], which can do a nonlinear fit to the magnetic measurements and an experimental pressure profile. The pressure profile used in this calculation was constructed from soft x-ray data. Fig. 5 shows the SXR profile and the result of the fit by IDENTC. Also shown is a normalized electron pressure profile obtained from interferometer electron density measurements and ECE

electron temperature measurements. Ion temperature profiles are not available for this discharge.

The ballooning stability analysis was done with the HBT equilibrium and stability code. To model the experimental pressure gradient more accurately, we use a spline fit of the normalized pressure profile from the interferometer and ECE in the equilibrium. The total pressure is adjusted, keeping the normalized pressure profile constant, so that the correct value of the poloidal beta is obtained. The q-profile (see Fig. 6) is taken from a fit with IDENTC, giving a value of q at the boundary of 3.2, and a value of q on axis of 0.95. The shape of the double x-point plasma boundary, resulting from the IDENTC fit, is approximated by prescribing the values of the ellipticity and the triangularity.

The result of the ballooning stability calculation is shown in a s-α diagram [shear $s = 2(\psi/q)\,(dq/d\psi)$ versus normalized pressure gradient $\alpha = -(4\mu_0 q^{*2}/\varepsilon B^2)\,\sqrt{\psi}\cdot dp/d\psi$ with $q^* = \varepsilon L B_0/\mu_0 I$, where L is the circumference of the plasma boundary] in Fig. 7. Drawn are the equilibrium curve and the boundary of the first region of stability. The latter boundary is calculated by increasing the total pressure, keeping the shape of the pressure and the q-profile constant. It is clear that the region of the plasma with the largest pressure gradients is close to the ballooning limit. The width of this region is about 15 cm. The error bars in this case are at least 15%.

In view of the fact that $\beta/\beta_{Troyon} = 65\%$ in this discharge and that the ballooning limit is approached in a region of only 15 cm width and with a minor radius of 1.10 m, it is interesting to see what the maximum beta is if the pressure profile is marginally stable to ballooning modes in the whole plasma. To calculate this marginal pressure profile, we start from the experimental pressure and the q-profile. Then, the pressure gradient is increased in small steps up to the ballooning limit, while keeping the q-profile constant. To avoid equilibria with a finite current density at the edge, which are likely to be unstable to external kink modes, the pressure gradient is optimized in the region $0.0 < \psi < \psi_m$, with $\psi_m = 0.90\text{-}0.95$. The resulting marginally stable profile of the pressure gradient $\alpha = -(4\mu_0 q^{*2}/\varepsilon B^2)\,\sqrt{\psi}\cdot dp/d\psi$ versus the normalized flux $\psi = (\Phi-\Phi_0)/(\Phi_1-\Phi_0)$ is shown in Fig. 8 (dotted line). The experimental profile is also shown (full line). Again, this shows that the discharge is close to marginal stability in the region $0.74 < \sqrt{\psi} < 0.84$. The small shear in the plasma center ($0.0 < \sqrt{\psi} < 0.45$) is the cause for the small maximum pressure gradient in the center. This behavior is also clear from the s-α diagram; the maximum gradient is following the boundary of the first region of stability of Fig. 7, which for $q_0 < 1.0$ starts at the origin.

The pressure profile that corresponds to the marginal pressure gradient is shown in Fig. 9. The toroidal beta of this equilibrium is 7.0%. Because of the low shear in the plasma center,

no significant pressure gradient can be sustained there. This leads to a marginally stable pressure profile with a similar shape as the experimental profile The large gradient near the edge of the plasma up to $\psi = 0.95$ causes a negative current sheet on the inside. This can be avoided by limiting the pressure gradient near the edge (the maximum gradient then occurs at $\psi = 0.90$). The toroidal beta drops to 6.3% in that case, which still corresponds to $3.4\ I / B_0 a$.

B. PEAKED PRESSURE PROFILES (DISCHARGES #20272 AND #20302)

The high beta shots, that will be discussed in this section, show clear signs that a beta limit is reached in these discharges. The maximum β does not increase when a larger heating power is applied and the loss of confinement is probably caused by the large MHD activity. The values of beta are at about 100% of the Troyon limit.

In the following we will discuss two discharges in more detail. The first is characterized by a pressure profile with an almost constant gradient over the minor radius. In the second discharge the peaking of the pressure profile is increased in the center by the injection of a pellet at the moment when the additional heating was switched on.

1. 'Triangular' pressure profile (discharge #20272)

The traces of the toroidal beta and the total heating power of the high beta discharge #20272 are shown in Fig. 10. At $t = 52.5$ s the maximum beta reaches 85% of the Troyon limit ($I = 2.09$ MA, $B_0 = 1.22$ T, $a = 1.11$ m, $\beta_P = 0.65$). Together with the clipping of beta, fishbone activity with toroidal mode number $n = 1$ and poloidal mode number $m = 1$ and 2 and ELMs are observed. The correlation of the beta clipping with the MHD activity is illustrated in Fig. 11. Here the MHD activity for $n = 1$ to $n = 4$ and the H-α signal, illustrating the ELM activity, is shown. After the drop in beta at $t = 52.25$ s, there is a phase up to 52.5 s with relatively small MHD activity in which β rises steadily towards its maximum value. The electron pressure profile at maximum beta, as measured by the LIDAR diagnostic, is shown Fig. 12. The pressure gradient is almost constant along the minor radius with a larger gradient in the plasma center.

The equilibrium at the maximum beta is reconstructed using the pressure profile of Fig. 12. The shape of the plasma boundary and the q-profile are taken from the fit by IDENTC of the equilibrium to the magnetic data and the pressure profile. In Fig. 12 we have indicated the actual pressure profile of the reconstructed equilibrium. The local disturbances of the profile, probably due to MHD activity, are smoothed out. By taking this normalized profile and scaling it up to the correct value of the poloidal beta, the contribution of the fast particles to the total

pressure is included. The profile shape of the fast particles is not known. In the ballooning stability analysis the possible stabilizing effect of the fast particles is not taken into account. The q-profile is shown in Fig. 13.

Ballooning stability analysis of this equilibrium yields a ballooning unstable region in the plasma center of about 50 cm centered around the magnetic axis. In Fig. 14 the normalized pressure gradient $\alpha = -(4\mu_0 q^{*2}/\varepsilon B^2)\ \sqrt{\psi}\cdot dp/d\psi$ in the plasma center ($0 < \psi < 0.1$) is shown as a function of the normalized flux $\psi = (\Phi-\Phi_0)/(\Phi_1-\Phi_0)$. Also shown is the pressure gradient that would be marginally stable to ballooning modes. This pressure gradient is determined by decreasing the pressure gradient in the unstable region only ($0.14 < \sqrt{\psi} < 0.26$) while other parameters are kept constant. This shows that the experimental pressure gradient at its maximum exceeds the ballooning limit by a factor of 1.5.

A possible explanation within the framework of ideal MHD could be that q on axis is much larger than 1.0. In that case there is, for low values of the shear, no unstable region between the first and the second region of stability and the pressure gradient can become arbitrarily large [19]. However, in view of the fact that fishbones with $^m/_n = {}^1/_1$ are observed, it is likely that q on axis is close to 1.0.

A different q-profile that could stabilize the large gradients in the center, but with q on axis near or below one, has a large enough negative global shear in the plasma center [20]. In this case there is a stability boundary in the center but it lies at higher values of the pressure gradient . We will return to this in the next section.

The unstable region near the origin in the s-alfa diagram could also be stabilized by non-ideal MHD effects like stabilization by fast particles [21], or stabilization of the large mode numbers of the ballooning instability in the plasma center by finite Larmor radius effects [22].

In the same way as for the discharge with the broad pressure profile, we calculated the profile that is marginally stable to ballooning modes for this discharge. The resulting profile of the pressure gradient versus the normalized flux is shown in Fig. 15. It shows that, apart from the instability in the center, the experimental pressure profile is close to the ballooning boundary in the region $0.08 < \psi < 0.30$. Thus, the discharge is exceeding or approaching the ballooning stability limit in a region of more than 40% of the minor radius of the plasma ($-0.36\ a < r < 0.59\ a$).

The pressure profile of the marginally stable equilibrium is shown in Fig. 16. The maximum toroidal beta is about 6.3%, which corresponds to $4.0\ I_p/B_0\ a$. The shape of the profile is triangular, like the experimental profile, however with the largest gradients on the outside instead of in the center. This is caused by the relatively large shear in the plasma center

which increases towards the plasma boundary The toroidal current density of this equilibrium has a negative current sheet on the inside of the plasma. Optimizing the pressure profile with the constraint of a positive current density will give a lower toroidal beta.

2. Peaked pressure profile with pellet injection (discharge #20302)

The peakedness of the pressure profile can be enhanced even further with the injection of a pellet in the plasma center. This was done in discharge #20302. At t = 51.0 s a 4 mm pellet was injected and 14 MW of neutral beam heating power was switched on. Traces of the toroidal beta and the total heating power are shown in Fig. 17. This discharge reaches a maximum beta of 0.03, which corresponds to 80% of the Troyon limit (I_p = 2.1 MA, B_0 = 1.4 T, a = 1.07 m, β_P = 0.70). In contrast to the previous discharge, there is no clipping of beta but a saturation associated with the onset of ELM activity. During the discharge a n = 1 mode is present, whose amplitude is growing with beta, causing an oscillation of the plasma center. A beta collapse occurs at t = 51.8 s at the maximum of the n = 1 and n = 2 mode activity when the modes lock.

The electron pressure profile at t = 51.5 s during the beta saturation phase is shown in Fig. 18. The ion pressure profile obtained from the ion temperature from the charge exchange diagnostic and the electron density profile has the same shape as the electron pressure profile. Again the contribution of the fast particles is included in the total pressure.

For the equilibrium reconstruction we use the electron pressure profile from Fig. 18. Information on the q-profile is obtained from soft x-ray data. Subtraction of two SXR intensity profiles at times of opposite phase of the MHD oscillation results in a 'displacement' as a function of the minor radius. The q-profile was taken such that the q = 1, 2 and 3 surfaces coincide with the different maxima of the displacement. The resulting q-profile is shown in Fig. 19.

The result of the ballooning mode analysis is shown in Fig. 20. Again the equilibrium profiles of the experimental and of the marginal pressure gradient are shown. Also in this discharge the measured pressure gradient exceeds the ballooning limit by a factor of two. The pressure profile that is marginally stable in the region where the experimental profile is unstable is indicated in Fig. 18. The marginal profile lies well outside the error bars of the measured electron pressure profile.

As mentioned in the previous section, changes in the q-profile may stabilize the large gradients in the plasma center. To check whether a large enough opening to the second region of stability appears when q on axis is increased, the ballooning unstable area as a function of q_0

was calculated (see Fig. 21). This shows that raising q_0 above one can stabilize part of the unstable region on the low shear side ($0.0 < \psi < 0.06$). At larger values of the shear, there remains a region where the maximum pressure gradient is limited by the first region of stability.

Another possible way of stabilizing the large gradients is to assume a non-monotonic q-profile with negative global shear in the region of the large gradients. The q-profile with which the pressure profile would be marginally stable is calculated by changing the q-profile in small steps, thereby slowly extending the region of negative shear and decreasing the shear in the center. This results in the q-profile shown in Fig. 22, where q on axis is 1.1 and the minimum value is 0.9. The non-monotonic q-profile requires a hollow current density profile (see Fig. 23). Current density profiles like this are unlikely if only the ohmic contribution to the total current is considered. However, the analysis with the TRANSP code (which solves the current diffusion equation in time) for previous pellet shots shows that the large gradients, caused by the strong additional heating after the injection of a pellet, give rise to a considerable contribution of the bootstrap current to the total current. This bootstrap current is peaked off axis creating a hollow current density profile similar to the profile of Fig. 23 [23].

C. CONCLUSIONS

The two types of high beta discharges produced at JET, that is discharges with broad and with peaked pressure profiles, have been shown to have very different properties with respect to ballooning mode stability. The stability limit is approached locally in both types of discharges.

In the evaluated discharge with the broad pressure profile and a q-profile which is flat or slightly hollow in the plasma center and has large shear near the edge, the maximum pressure gradient near the edge is close to the ballooning stability limit. The pressure profile that is marginally stable to ballooning modes, with the same q-profile, shows that higher beta values can be ballooning stable if the region with the large gradients can be extended to the plasma edge.

In the discharges with the peaked pressure profile, the large gradients in the plasma center exceed the ballooning stability limit by a factor of 1.5 to 2 if a monotonic q-profile is assumed. It must be noted that this instability is not caused by the low shear in the center, as was found in previous high beta discharges [24]. It was shown that the unstable region still exists when q on axis is increased from 0.9 to 1.4. Complete stabilization is possible with a non-monotonic q-profile with large negative shear in the center. The contribution of the bootstrap current can provide the hollow current density profile needed for this q-profile. Outside the unstable central part, the almost constant pressure gradient is just below the ballooning boundary over more

than 40 % of the minor radius. Also in the case of peaked pressure profiles higher values of beta, stable to ballooning modes, are possible if the pressure gradient on the outside of the plasma can be increased.

IV. SINGLE AND DOUBLE NULL X-POINT PLASMAS

In order to have a better control over the impurity content of the plasma, in the near future JET will operate with a divertor geometry with a single X-point. Also, during past high β operation both single and double X-point plasma shapes have been used (although the majority of high β discharges had a double X-point shape). Here, we study the effects of the change of the plasma shape from a double to a single X-point geometry on the ballooning mode stability properties of the plasma.

A. STABILITY OF UP-DOWN ASYMMETRIC EQUILIBRIA

The study of single X-point divertor discharges requires the handling of up-down asymmetric equilibria. To that end, we have extended the equilibrium and ballooning parts of HBT with the option to analyze asymmetric equilibria. This extension is fully documented in the accompanying report [8]. The present section is a first illustration of this new option, which may be extensively exploited for the study of future pumped divertor discharges.

The effect of non up-down symmetry may be understood as creating a difference in the triangularity between the upper and lower halves of the plasma. Since the influence of the triangularity on the MHD stability of up-down symmetric plasmas is relatively well known, we can estimate what the effect will be. Increasing the triangularity (i.e. changing the shape from an ellipse to a D shape) will cause an increase of the poloidal field on the outside of the torus, thereby decreasing the length of the field lines in the bad curvature region of the plasma. This will have a stabilizing effect on ballooning modes. For example, it was shown in [25] that the maximum β for ballooning modes increases linearly from $\beta = 3.5$ % to 4.5%, for the profiles considered, when the triangularity changes from 0.0 to 0.50.

Another effect of increasing the triangularity is that the corners at the top and bottom of the plasma boundary become less round. This will increase the total shear near the plasma boundary, which again has a stabilizing effect. Also, the local shear increases rather rapidly near the corners. The influence on the ballooning mode stability of the increase of the local shear is not obvious because the integrated local shear appears both in the stabilizing term of the field line bending and in the destabilizing term in connection with the tangential curvature.

Near the magnetic axis the influence of the triangularity is best illustrated by the Mercier criterion [26] :

$$q_0 \left\{ 1 - \frac{4}{3+\kappa^2} \left[\frac{3}{4} \frac{\kappa^2-1}{\kappa^2+1} \left(\kappa^2 - \frac{2\delta}{\varepsilon}\right) + \frac{(\kappa-1)^2}{\kappa(\kappa+1)} \beta_{p0} \right] \right\} > 1 , \qquad (4.1)$$

where κ is the ellipticity, δ is the triangularity, ε is the local inverse aspect ratio, and β_{p0} is the poloidal beta on axis. This implies that for $\kappa = 1.0$ the triangularity has no effect on the stability but for $\kappa > 1$ triangularity adds a stabilizing term.

B. INFLUENCE OF THE CHANGE FROM DOUBLE TO SINGLE X-POINT

In this section we will compare the ballooning stability properties of single and double null X-point plasma shapes. For a particular equilibrium with a double X-point shape, the marginally stable pressure profile is calculated. Then the plasma shape is changed to a single null X-point shape, while keeping the other equilibrium quantities the same, and the marginally stable pressure profile is calculated again. Comparison of these two marginally stable pressure profiles will then show what the influence is of the different shapes. The X-point shape is approximated with the appropriate value of the triangularity.

For the marginally stable equilibria with a double X-point shape, we use the equilibria of the high beta discharges of the previous paragraphs of which the marginally stable pressure profiles were calculated. Both the example with a broad pressure profile (discharge #19970) and the one with a peaked pressure profile (discharge #20272) will be discussed.

As an example of the different plasma boundaries, the two equilibria of discharge #19970 with a double and a single X-point are shown in Figs. 24a and 24b, respectively. The ellipticity of the plasma boundary is the same for both cases. The upper triangularity changes from 0.38 to 0.15 while the lower part of the plasma boundary is unchanged. The mentioned change in the local shear is illustrated in Figs. 25a and 25b. In this figure the local shear versus the poloidal angle is shown on the flux surface $\psi = 0.80$.

The result of the calculation of the marginal pressure profiles is shown Fig. 26. This picture shows the normalized pressure gradient α versus the normalized flux. The lower two curves in Fig. 26 correspond to the equilibrium with the broad pressure profile (#19970). The upper two curves correspond to the case with a triangular pressure profile (#20272). The two solid and dashed curves distinguish the double and single X-point plasma boundaries, respectively. For both cases, decreasing the upper triangularity also decreases the maximum pressure gradient that is stable to ballooning modes. This is consistent with the general stabilizing effect of adding triangularity. The figure also shows that the effect of changing from double to single X-point plasmas is rather small (< 10%) for typical JET parameters.

For low-n modes, the effect on the stability of different values for upper and lower triangularity may be different. Degtyarev et al. [27] have calculated marginally stable equilibria to both low-n and ballooning modes for typical ITER design parameters. They found that the external kink modes pose a stronger constraint on the maximum β for single X-point plasmas than for double X-point plasmas. When the symmetrical plasma has a triangularity of 0.4 and the asymmetrical plasma has triangularities of 0.2 and 0.6, the maximum β decreased from 6.0 to 4.5 %. How the situation changes for typical JET parameters remains to investigated.

V. EXTERNAL KINK MODES

In this section the results are presented of the analysis of external kink modes at high β. Since these modes are treated with the high-β ordering in the program HBT, some effort is needed to convert the experimental equilibrium data to the equivalent profiles that represent the dominant high-β part. Past experience with HBT [7] has shown that all important high-β physics effects, like the Troyon, Sykes, and Wesson scalings, are included but that the neglect of terms of higher order than ε^2 in the inverse aspect ratio may lead to some uncertainty with respect to modes that grow on a slower time scale. With this proviso, we will study external kink modes for the JET discharges treated without an ordering in the sections III and IV.

A. GLOBAL KINK MODES

Discharge #20272 has been investigated with respect to the high-β external kink limit. For reasons of accuracy, the outermost flux surfaces close to the separatrix have been eliminated in this study, effectively resulting in a less elongated cross-section. The adapted experimental profiles are shown in Fig. 27. Here we take q on axis to be slightly above one ($q_0 = 1.03$) in order to avoid the situation where the internal kink will limit the maximum beta. Especially in this discharge with a peaked pressure profile, this would lead to a low value of the β limit. A high-β scaling law for external kink modes is obtained by simultaneously pushing the value of $<\beta>$ and scanning the parameter q^*. For this discharge, we find the maximum beta limited by an external kink mode to be the same as the β value as given by the Troyon scaling law. This value is well below the maximum β limited by ballooning modes only (see par. III.B.2). However in that case in determining the maximum β we optimized the pressure profile with a constant q-profile whereas here we keep the shape of both profiles the same and increase the total pressure.

Typical high-β discharges in JET have q profiles with a value of q_0 around 1 and a value of $q_1 > 2$. Hence, one expects global kink modes with m = 1 and m = 2 components, where the m = 1 component will be largely internal, whereas the external part will have a dominant m = 2 contribution. This is confirmed by the flow pattern of the modes depicted in Fig. 28. Here we have chosen a mode which is at the border of the Troyon stability boundary. In Fig. 28a the mode is stabilized by putting a conducting shell at the plasma boundary. Consequently, the flow pattern just shows the m = 1 contribution of the internal kink mode. Removing the shell

leads to the coupled m = 1 and m = 2 mode pattern depicted in Fig. 28b. This pattern is typical for the pressure dominated kink modes which lead to the Troyon beta limit.

B. PEELING MODES

Edge localized modes (ELM's) are frequently observed on the various diagnostics during an H-mode phase. The occurrence of ELM's is associated with particle loss at the plasma boundary, thereby reducing the particle and energy confinement time. Hence, ELM's also reduce the impurity content of the plasma, so that they can be used for the production of long duration H-modes.

Both pre- and postcursors of ELM's have been observed on the magnetic signals. In ASDEX [28] as well as in JET [29], the precursors have a toroidal mode number n = 1. The corresponding poloidal mode numbers are relatively high, i.e. m = 3 - 4 in ASDEX and m = 5 - 10 in JET. In general, two types of ELM's can be distinguished, viz. giant ELM's and smaller ELM's of the so-called grassy variety. In DIII-D [30] it was shown that the occurrence of a giant ELM correlates well with the presence of a large pressure gradient at the plasma edge reaching the first stability boundary. This does not apply for the smaller ELM's. Also, it was shown in Ref. [31] that the current density near an X-point can cause considerable changes in the ballooning stability boundary.

It has recently been suggested [32] that ELM's may be manifestations of the so-called peeling mode [33]. This mode is a milder form of the external kink mode driven by a finite gradient of the current density at the plasma edge. The mode is characterized by a perturbation which is localized in a narrow region near the plasma boundary. From standard low-β tokamak theory [34] it is known that peeling modes may become unstable when a rational q-surface lies just outside the plasma boundary. Correspondingly, the unstable region in the parameter q_1 extends from integer values m down to a value $m - \Delta m$, where, for parabolic current density profiles, the width Δm of this region decreases with increasing m. The localization of the mode, i.e. whether the mode is a global external kink or a peeling mode localized at the plasma boundary, depends on the details of the shape of the toroidal current density profile. In Ref. [35] it was shown that, for finite aspect ratio plasmas with a circular boundary, the stability boundary remains qualitatively the same, but there is a quantitative change due to the dependence of the current profile on the aspect ratio.

To study the relevance of peeling modes for plasma conditions at JET we have investigated the peaked pressure equilibrium of discharge #20272 again. In order to be able to distinguish between the pressure dominated kinks, studied in the previous section, and the

current driven peeling modes, we have lowered the value of the poloidal beta to half of its original value. This is justified by the the fact that ELM's are observed at low values of $<\beta>$. Furthermore, in order to excite the peeling mode, we have artificially added a finite current density at the plasma edge.The resulting current density and q-profiles are shown in fig. 29. The low-n stability (n=1) of this equilibrium was then calculated by scanning for the growth rate as a function of q^*. By varying q^* we also varied the value of q_1 (from 3.2 down to 2.5) while keeping the ratio q_1/q_0 constant. However, to our surprise, no peeling mode was found in this manner. The equilibria turned out to be stable for all values of q considered. Also, the mode structure of the stable modes in this region did not show any localized peeling mode features.

Since peeling modes are easily excited in a circular plasma, we then changed the plasma shape of the original equilibrium to a circular one, while keeping the other parameters the same. As expected, for this case the equilibrium becomes unstable to m = 3, n = 1 peeling modes when $q_1 < 3$. An example of the flow field of these modes is shown in Fig. 30a. Increasing the elongation of the plasma cross-section by changing the ellipticity from 1.0 to 1.2 basically leaves the mode structure unchanged, as shown in fig. 30b (where one should recall that the sign of a linear mode has no physical meaning) but the growth rate is drastically reduced. For JET relevant values of the ellipticity (ellipticity > 1.4) the mode turns out to be completely stable.

Consequently, our first conclusion is that peeling mode might be less important in elongated plasmas like JET, as compared to circular plasmas like TFTR.

Acknowledgements

We would like to acknowledge contributions of E. Lazzaro and P. Smeulders and discussions with D. O'Brien, D. Campbell, T. Hender, O.J. Kwon, J. O'Rourke, P. Stubberfield, and J. Wesson. This work was performed under JET contract nº JT9/9003 with financial support from NWO, EURATOM, and JET.

References

[1] Smeulders P.and the JET team (1989), APS Meeting, 13-17 November, 1989, also presented at the ITER Meeting on Beta Limits and Profiles, Garching, March, 1990.
"High-beta Regimes in JET".

[2] Kardaun O., Thomsen K., Christiansen J., Cordey J., Gottardi N., Keilhacker M., Lackner K., Smeulders P., the JET team (1989), 16th EPS Conf. on Plasma Physics and Contr. Fusion, Vol. I, p. 253.
"On Global H-mode Scaling Laws for JET".

[3] Goedbloed J.P. (1981), Comp. Phys. Commun. **24**, 311.
"Conformal Mapping Methods in Two-dimensional Magnetohydrodynamics".

[4] Galvão R.M.O., Goedbloed J.P., J. Rem, P.H. Sakanaka, T. Schep, and M. Venema (1982), Proc. 9th International IAEA Conf. on Plasma Physics and Contr. Nucl. Fusion Research, Baltimore, Vol. III, p. 3, IAEA , Vienna, 1983.
"Global Kink and Ballooning Modes in High-beta Systems and Stability of Toroidal Drift Modes".

[5] Goedbloed J.P. (1984), Comp. Phys. Commun. **31**, 123.
"Some Remarks on Computing Axisymmetric Equilibria";
Goedbloed J.P. (1986), Comp. Phys. Commun. **41**, 196.
"Erratum notice".

[6] Galvão R.M.O. (1984), in *Radiation in Plasmas* ,ed. B. McNamara, World Scientific, Singapore, Vol. I, p. 280.
"Magnetohydrodynamic Theory of High-beta Diffuse Plasmas".

[7] Goedbloed J.P., Hogewey G.M.D., Kleibergen R., Rem J., Galvão R.M.O., Sakanaka P.H. (1984), Proc. 10th International IAEA Conf. on Plasma Physics and Contr. Nucl. Fusion Research, London, Vol. II, p. 165, IAEA , Vienna, 1985.
"Investigation of High Beta Tokamak Stability with the Program HBT".

[8] Huysmans G.T.A., Galvão R.M.O., and Goedbloed J.P. (1990), Rijnhuizen Report 90-194.
"Documentation of the High-beta Stability Codes HBT and HBTAS at JET".

[9] H. Saurenmann, S. Semenzato, R. Gruber, and F. Troyon (1982), Proc. 9th International IAEA Conf. on Plasma Physics and Contr. Nucl. Fusion Research, Baltimore, Vol. III, p. 17, IAEA , Vienna, 1983.
"Regimes of Operation of JET and INTOR Compatible with Ideal MHD Stability Requirements".

[10] Troyon F., Gruber R., Saurenmann H., Semenzato S., and Suci S. (1984), Plasma Physics and Controlled Fusion **26**, 209.
"MHD-limits to Plasma Confinement".

[11] Sykes A., Turner M.F., Patel S. (1983), Proc. 11th Conf. on Controlled Fusion and Plasma Physics, Aachen, EPS , Vol. II, p.363.
"Beta Limits in Tokamaks Due to High-n Ballooning Modes".

[12] Wesson J.A. and Sykes A., Nuclear Fusion (1985) **25**, 85.
"Tokamak Beta Limit".

[13] D'Ippolito D.A., Freidberg J.P., Goedbloed J.P., and Rem J. (1978), Physics of Fluids **21**, 1600.
"High-beta Tokamaks Surrounded by Force-free Currents".

[14] Soltwitsch H., Stodiek W., Manickam J., Schlüter J., Plasma Physics and Controlled Nuclear Fusion Research. 1986, Proceedings of the 11th International Conference, Kyoto (IAEA, Vienna, 1987), Vol. 1, p. 263.
"Current Density Profiles in Textor Tokamak".

Campbell D.J.et al. (1988), Phys Rev. Lett. Vol. 60, p. 2148.
"Stabilization of Sawteeth with Additional Heating in the JET Tokamak"

[15] Goedbloed J.P. and Sakanaka P.H. (1974), Physics of Fluids **17**, 908.
"New Approach to Magnetohydrodynamic Stability: I. A Practical Stability Concept".

[16] Lazzaro E., Tanga A., Huysmans G., O'Brien D., von Hellerman M., to be published.
"H-mode Confinement at Low q and High Beta in JET".

[17] Stambaugh R. et al. (1988), Plasma Physics and Controlled Fusion, Vol. 30, nº. 11 p. 1585.
"High Beta and ECRH Studies in DIII-D"

[18] Blum J., Gilbert J.C., Le Foll J., Thooris B. (1986), 8th Europhysics Conf. on Computational Physics: Computing in Plasma Physics, Eibsee, Vol. 10D, p. 49.
"Numerical Identification of the Plasma Current Density in a Tokamak from the Experimental Measurements".

[19] Antonsen A., Basu B., Coppi B., Crew G., Englade R., Ferreira A., Lane B., Pegoraro F., Porkolab M., Ramos J.J., Sharkey N., Sugiyama L. (1980), Plasma Physics and Contr. Nucl. Fusion Research 1980, Vol. I, p. 83, IAEA-CN-38/C-3.
"Confinement and Heating of High Density Plasmas".

[20] Greene J.M., Chance M.S. (1981), Nucl. Fusion **21**, 453.
"The Second Region of Stability against Ballooning Modes".

[21] Rosenbluth M.N., Tsai S.T., Van Dam J.W., Engquist M.G. (1983), Phys. Rev. Lett. Vol. 51, p. 1967.
"Energetic Particle Stabilization of Ballooning Modes in Tokamaks".

[22] Hastie R.J., Hesketh K.W. (1981), Nucl. Fusion **21**, 651.
"Kinetic Modifications to the MHD Ballooning Mode".

[23] Stubberfield P.M., Balet B., Campbell D., Challis C.D., Cordey J.G., Hammett G., O'Rourke J., Schmidt G.L. (1989), 16th EPS Conf. on Plasma Physics and Contr.

Fusion, Vol. I, p. 253.
"Current Density Profile Evolution in JET".

[24] Huysmans G.T.A., Galvão R.M.O., Goedbloed J.P., Lazzaro E., Smeulders P. (1989) JET-P(89) 34.
"Ballooning stability of JET discharges".

[25] Todd A.M.M., Manickham J., Okabayashi M., Chance M.S., Grimm R.C., Greene J.M., Johnson J.L. (1979), Nucl. Fusion **19**, 743.
"Dependance of Ideal-MHD Kink and Ballooning Modes on Plasma Shape and Profiles in Tokamaks".

[26] Friedberg J.P. (1987), Plenum Press, New York,
"Ideal Magnetohydrodynamics".

[27] Degtyarev L.M., presented at the ITER meeting on Beta Limits and Profiles, Garching, March 1990.
"Shear and Pressure Profile Effects on Ideal Ballooning Modes Stability".

[28] Toi K., Gernhardt J., Kluber O., and Kornherr M.(1989), Phys. Rev. Lett., Vol. 62, p. 430
"Observation of Precursor Magnetic Oscillations to the H-mode Transition of the ASDEX Tokamak".

[29] Joffrin E.H. et al. (1989), 16th EPS Conf. on Plasma Physics and Contr. Fusion, Vol. I, p. 225.
"An Interpretation of the Structure of ELMs and the H to L Transition on JET".

[30] Gohil P., Ali Mahdavi M., Lao L., Burrel K.H., Chu M.S., DeBoo J.C., Hsieh C.L., Ohyabu N., Snider R.T., Stambaugh R.D., and Stockdale R.E. (1988), Phys. Rev. Lett. Vol. 61, p. 1603.
"Study of Giant Edge-localized Modes in DIII-D and Comparison with Ballooning Theory".

[31] Bishop C.M., Kirby P., Connor J.W., Hastie R.J., and Taylor R.B. (1984), Nucl. Fusion **24**, 1579.
"Ideal MHD Ballooning Stability in the Vincity of a Separatrix".

[32] Manickam J., presented at the ITER meeting on Beta Limits and Profiles, Garching, March 1990.
"The Role of Ideal Modes in Experiments".

[33] Frieman E.A., Greene J.M., Johnson J.L., and Weiner K.E. (1973), Physics of Fluids, Vol. 16, p.1108.
"Toroidal Effects on Magnetohydrodynamic modes in Tokamaks".

[34] Wesson J.(1978), Nucl. Fusion **18**, 87.
"Hydromagnetic Stability of Tokamaks".

[35] Turnbull A.D., and Troyon F. (1989), Nucl. Fusion **29**, 1887.
"Toroidal Effects on Current Driven Modes in Tokamaks".

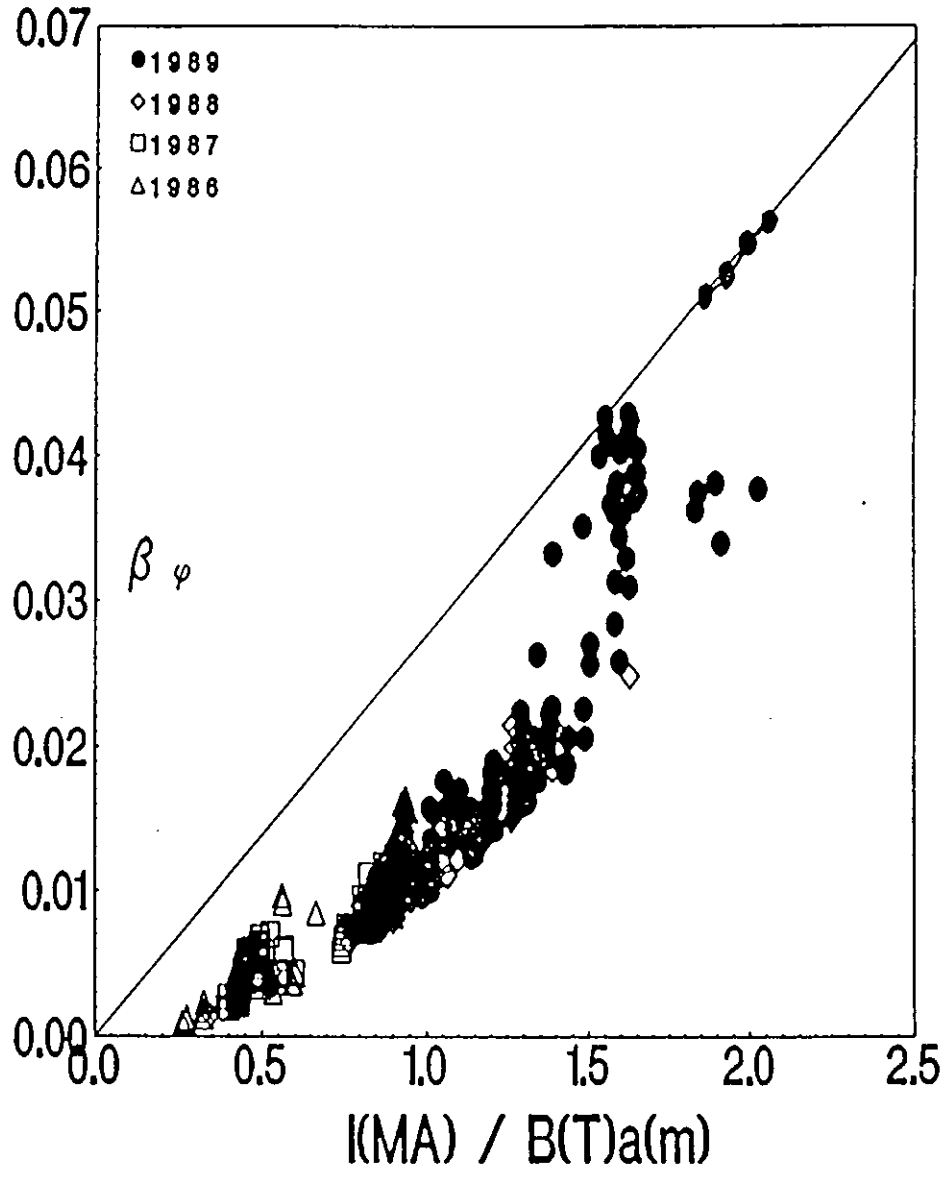

Fig. 1 Toroidal beta of JET high-beta discharges with $\beta_p > 0.3$ as a function of the normalized current. Included is the Troyon limit (full line).

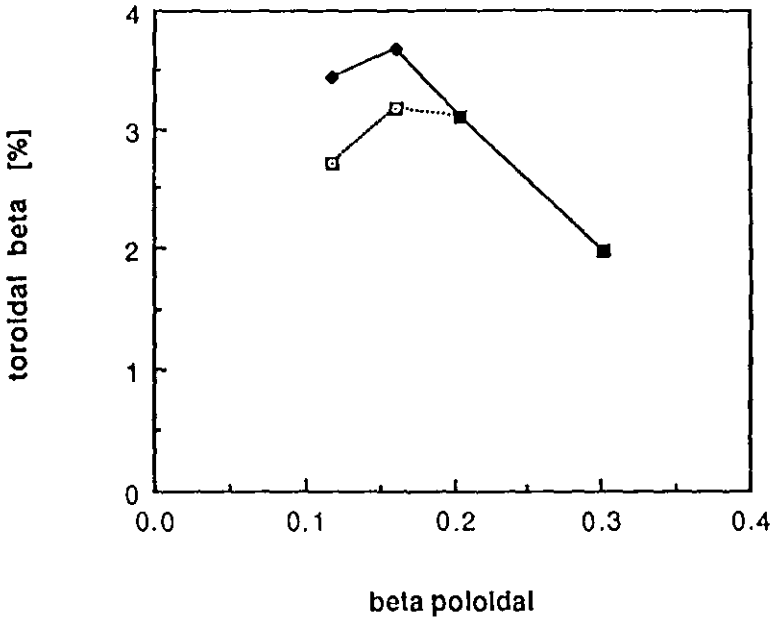

Fig. 2 Comparison of β values as a function of the poloidal beta, optimized for ballooning modes, with the instability at q_0 taken into account (dashed, lower curve) and without this instability (full, upper curve).

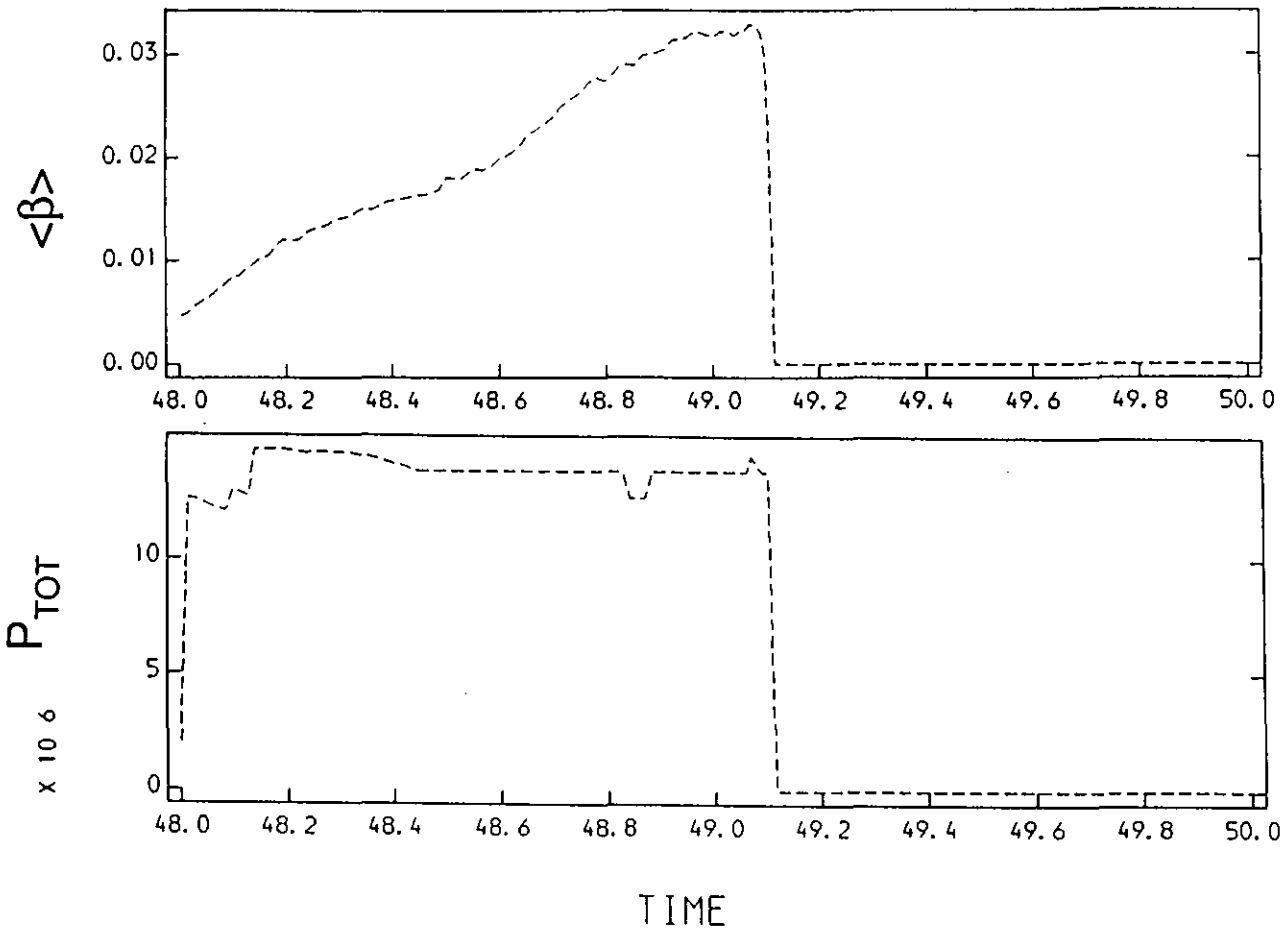

Fig. 3 Traces of the toroidal beta and the total heating power of discharge #19970.

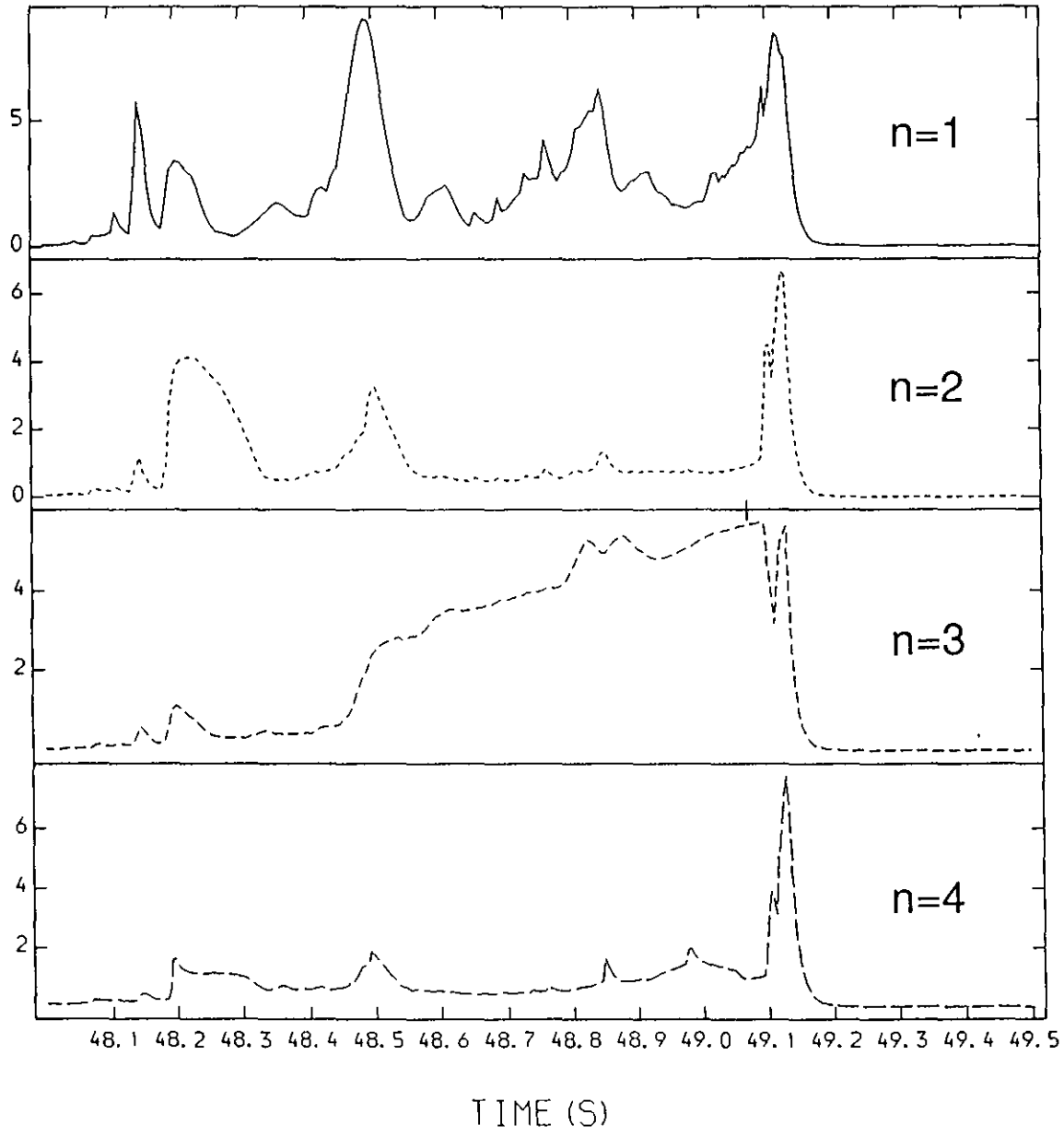

Fig. 4 The MHD activity during discharge #19970 for toroidal modenumbers n = 1 - 4.

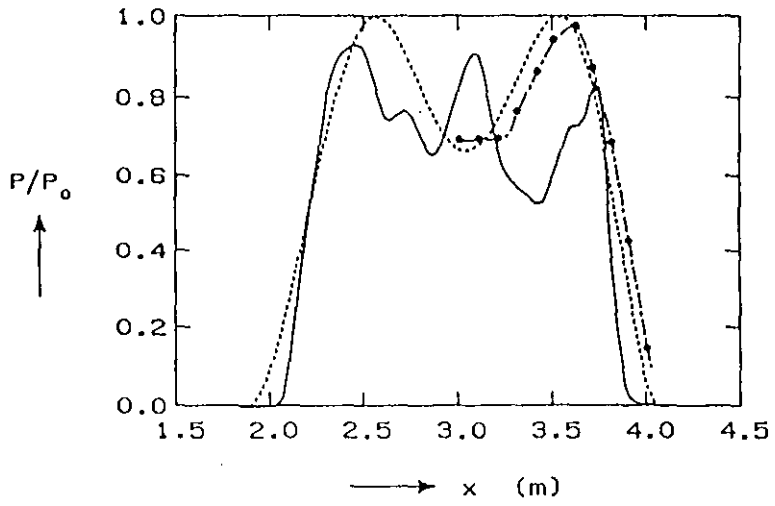

Fig. 5 Pressure profile of discharge #19970 at t = 49.0 s from SXR data (full line), from interferometer and ECE data (o-o line), and the fit by IDENTC (dotted line).

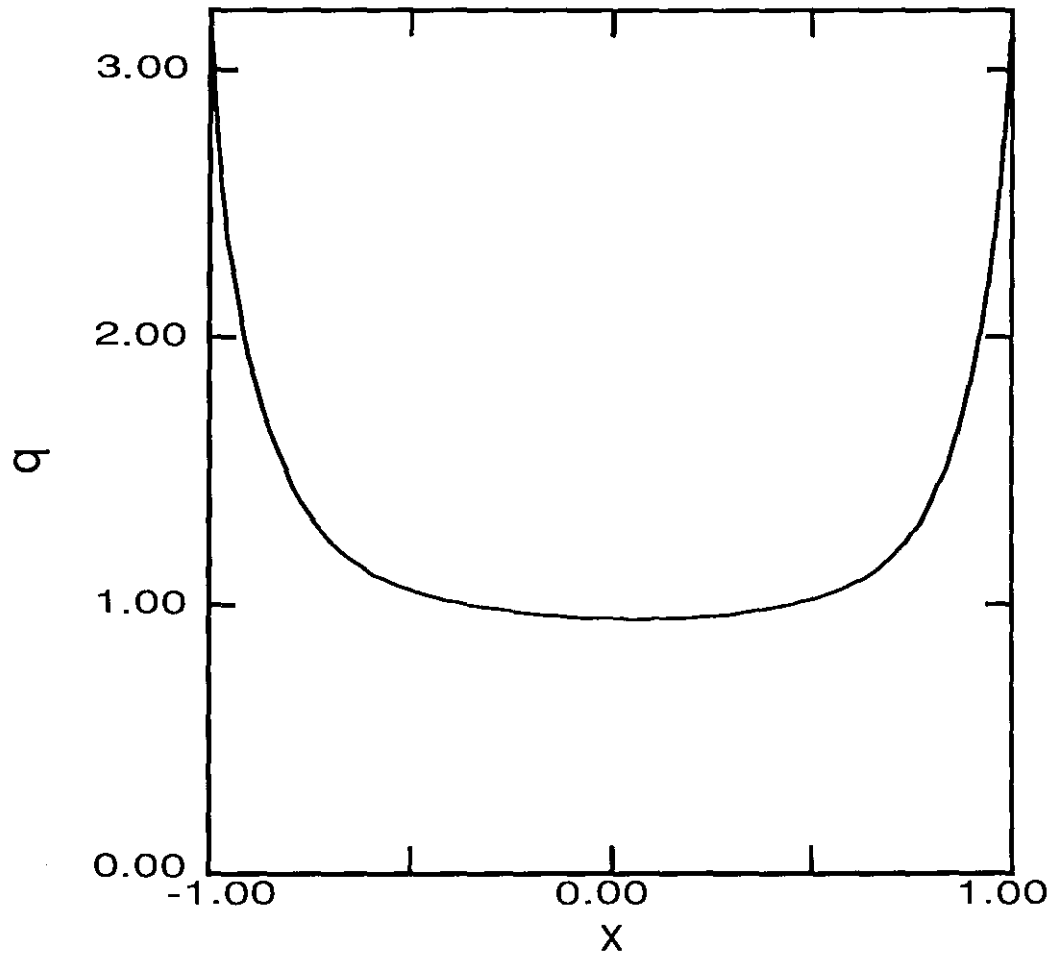

Fig. 6 The q-profile of the reconstructed equilibrium of discharge #19970 at t = 49.0 s..

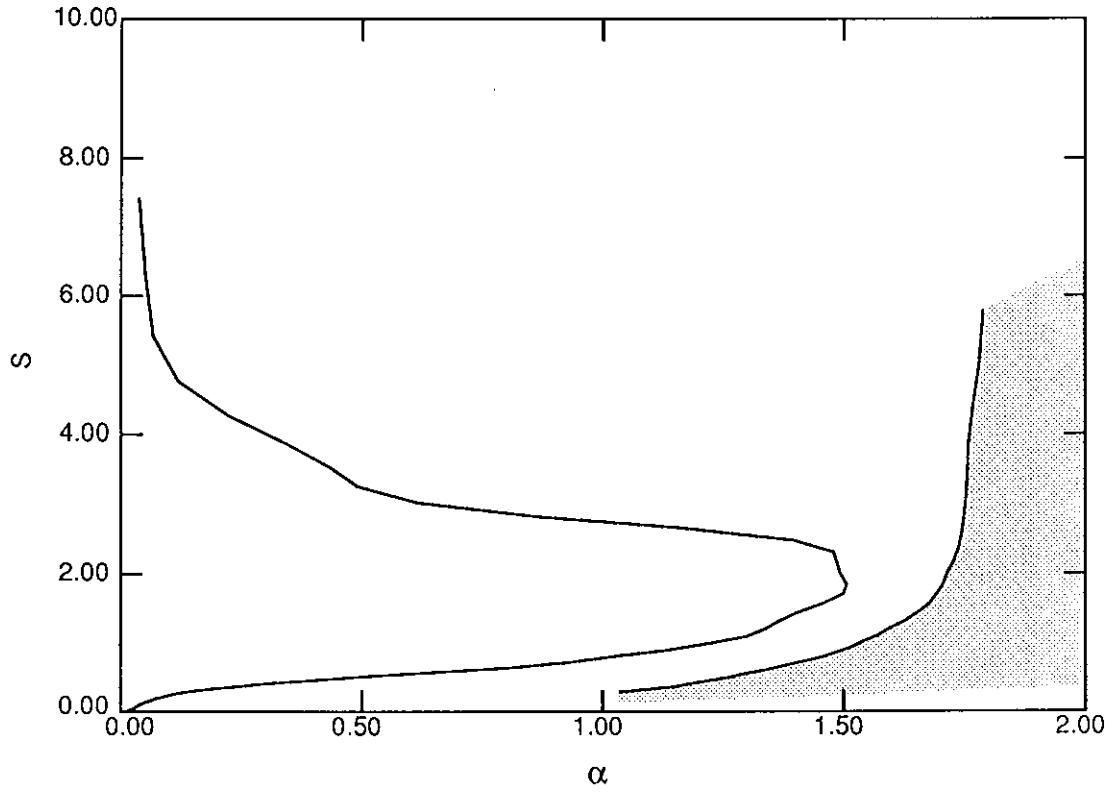

Fig. 7 The shear (s) versus the normalized pressure gradient (α) for discharge #19970, t = 49.0 s. The shaded area indicates the ballooning unstable region where the full curve of the area is the calculated part of the boundary of the first region of stability.

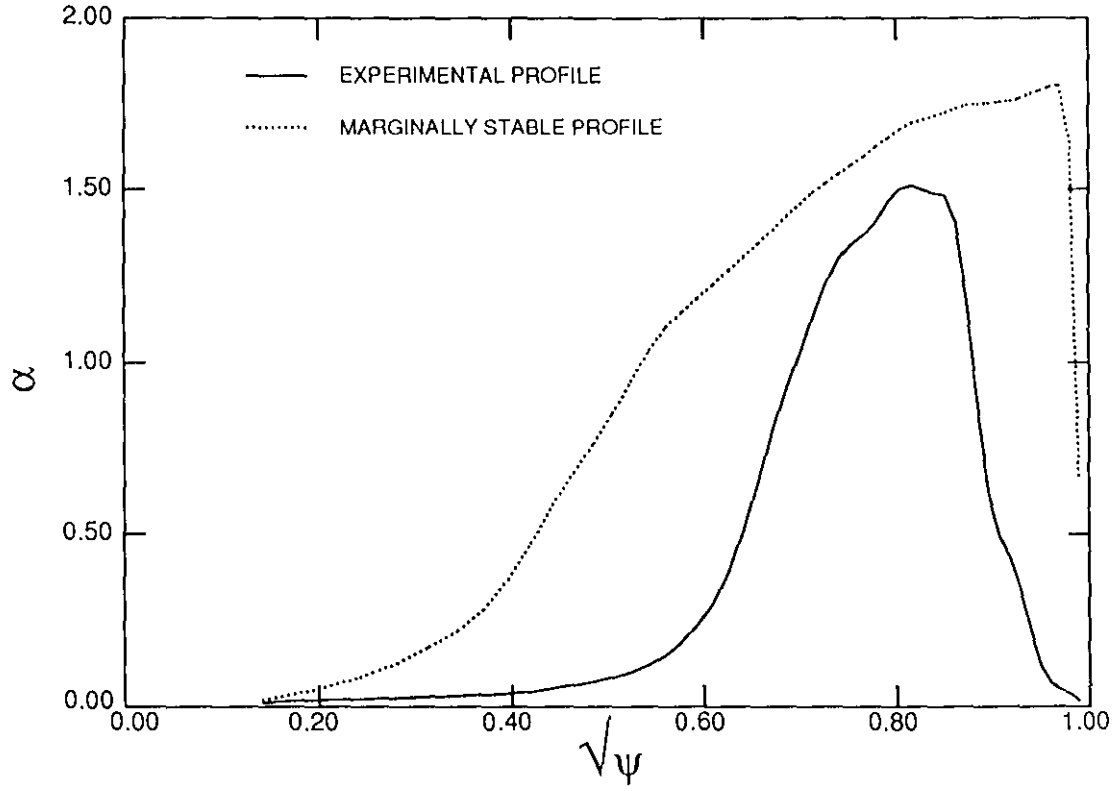

Fig. 8 The normalized pressure gradient of the marginally stable equilibrium and of the experimental equilibrium as a function of the normalized flux of discharge #19970, t = 49.0 s.

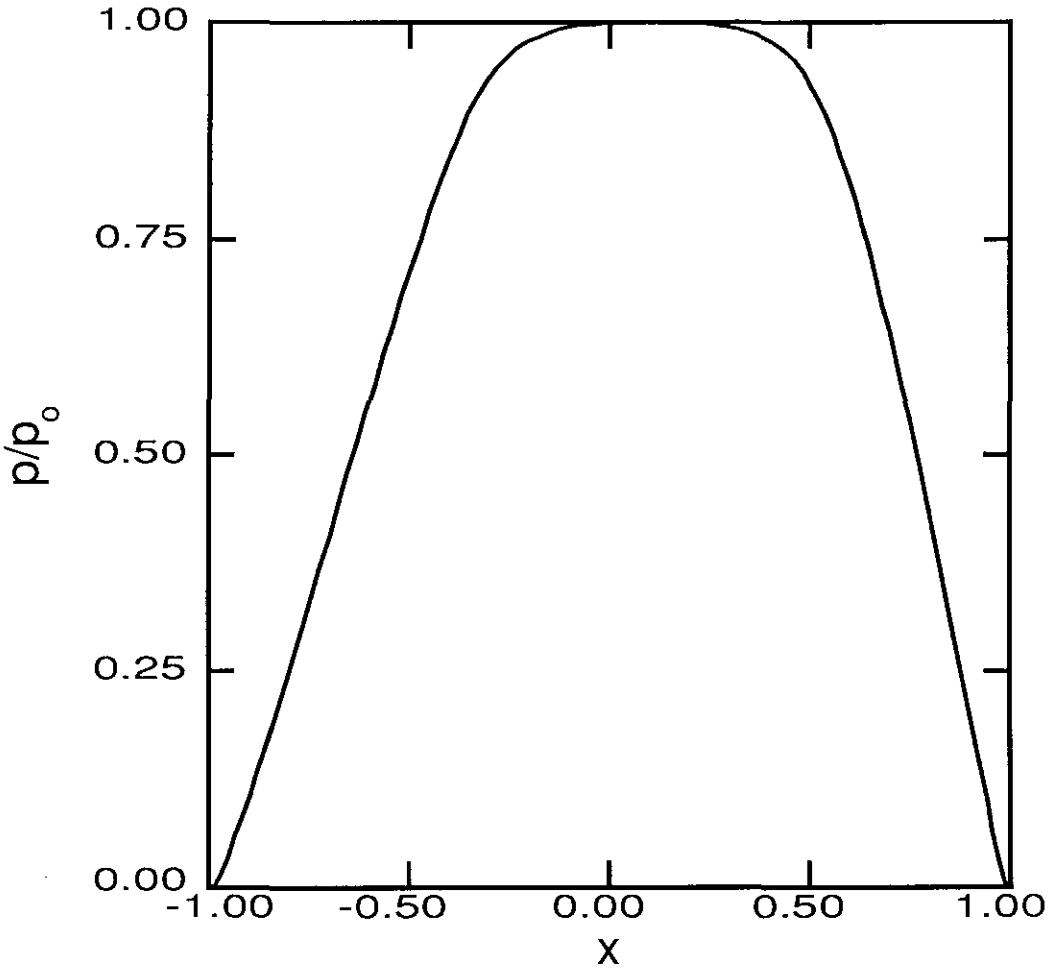

Fig. 9 The pressure profile corresponding to the marginally stable pressure gradient profile of Fig. 7.

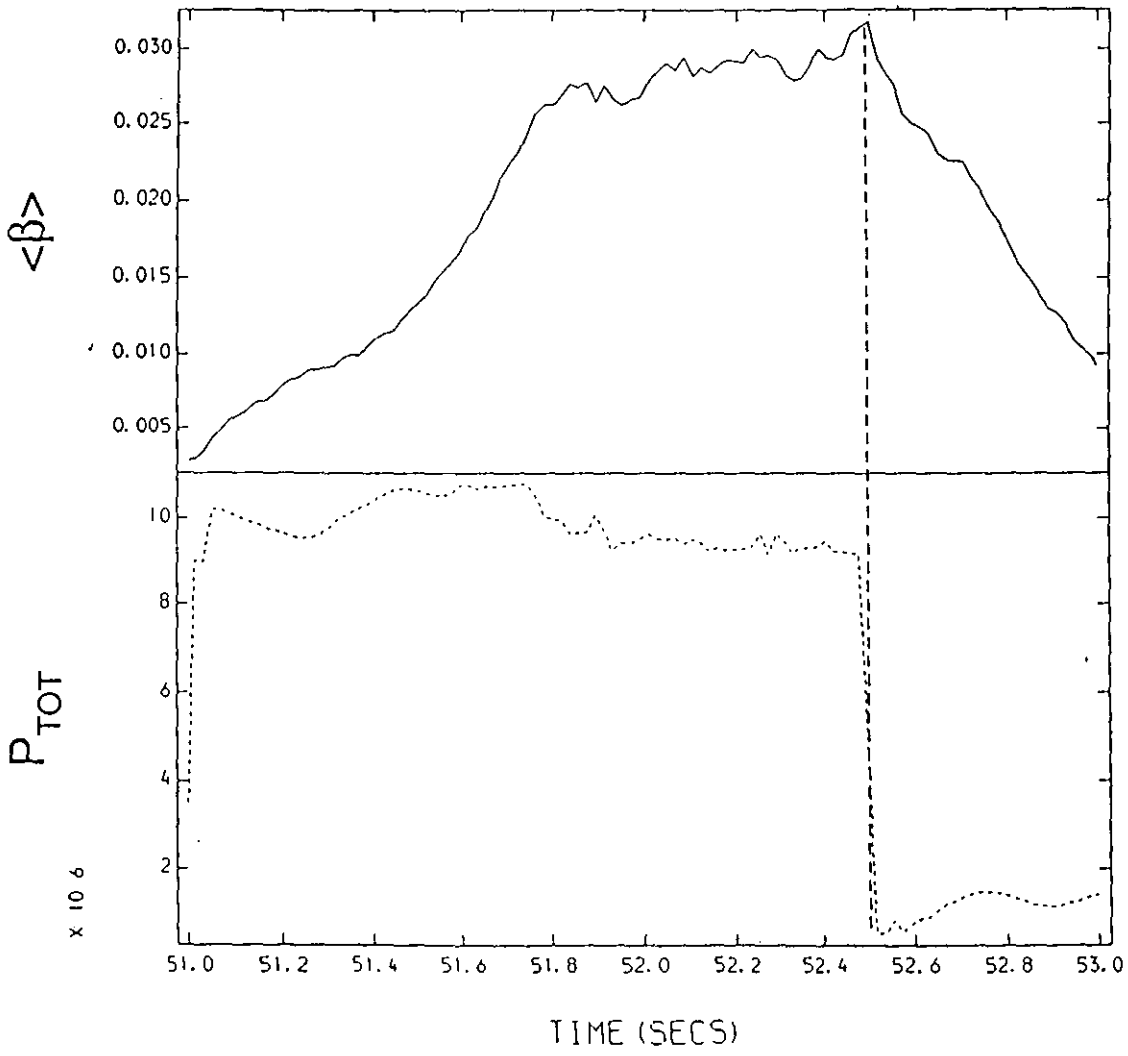

Fig. 10 The toroidal beta and the total heating power of discharge #20272.

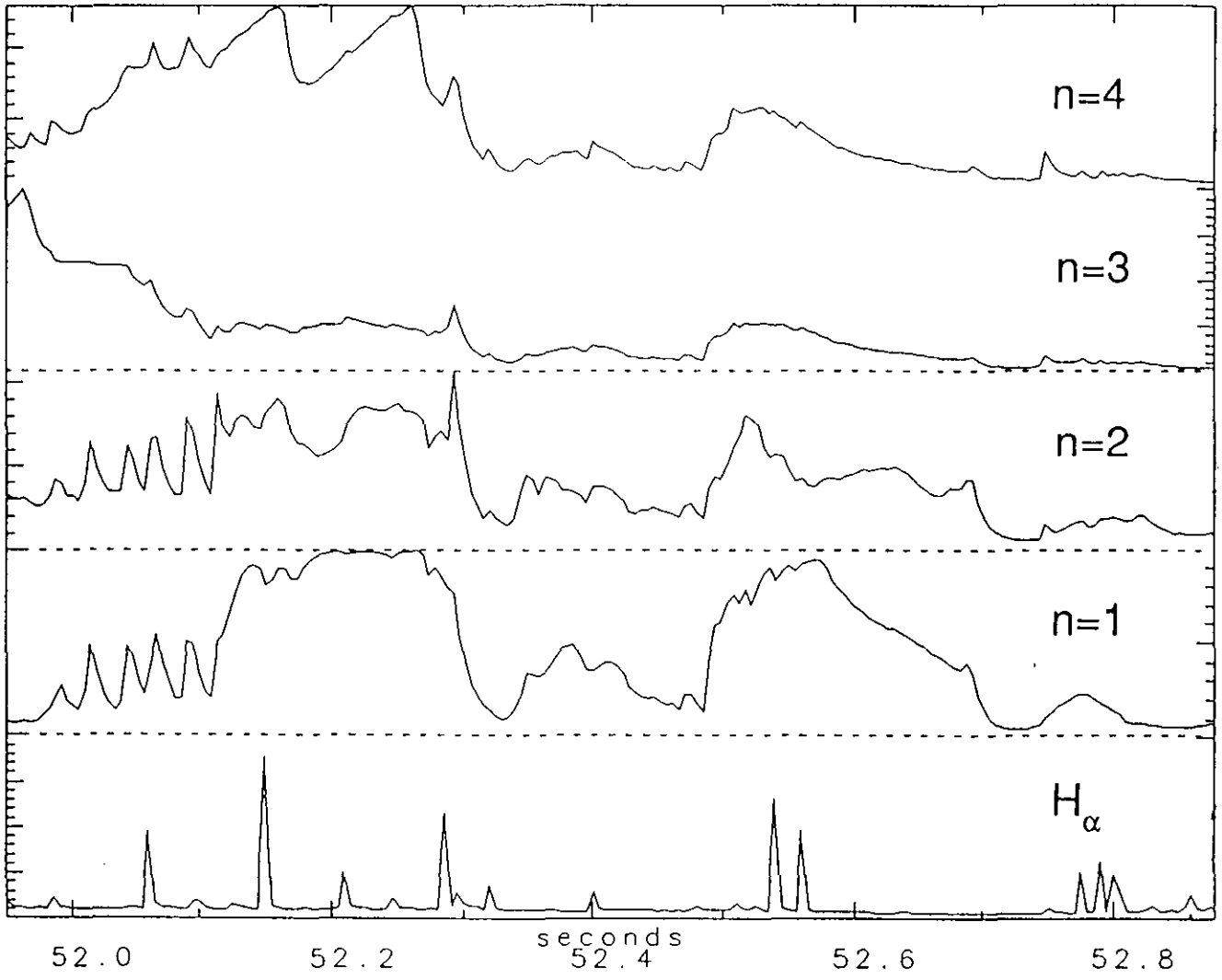

Fig. 11 The MHD activity during discharge #20272.

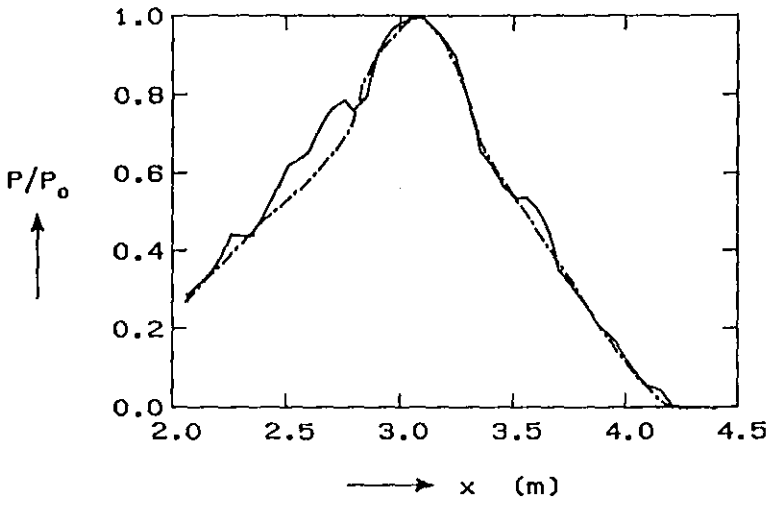

Fig. 12 The pressure profile of discharge #20272 at the time of maximum beta (t = 52.5 s). Included (dashed curve) is the smoothed pressure profile used in the equilibrium reconstruction.

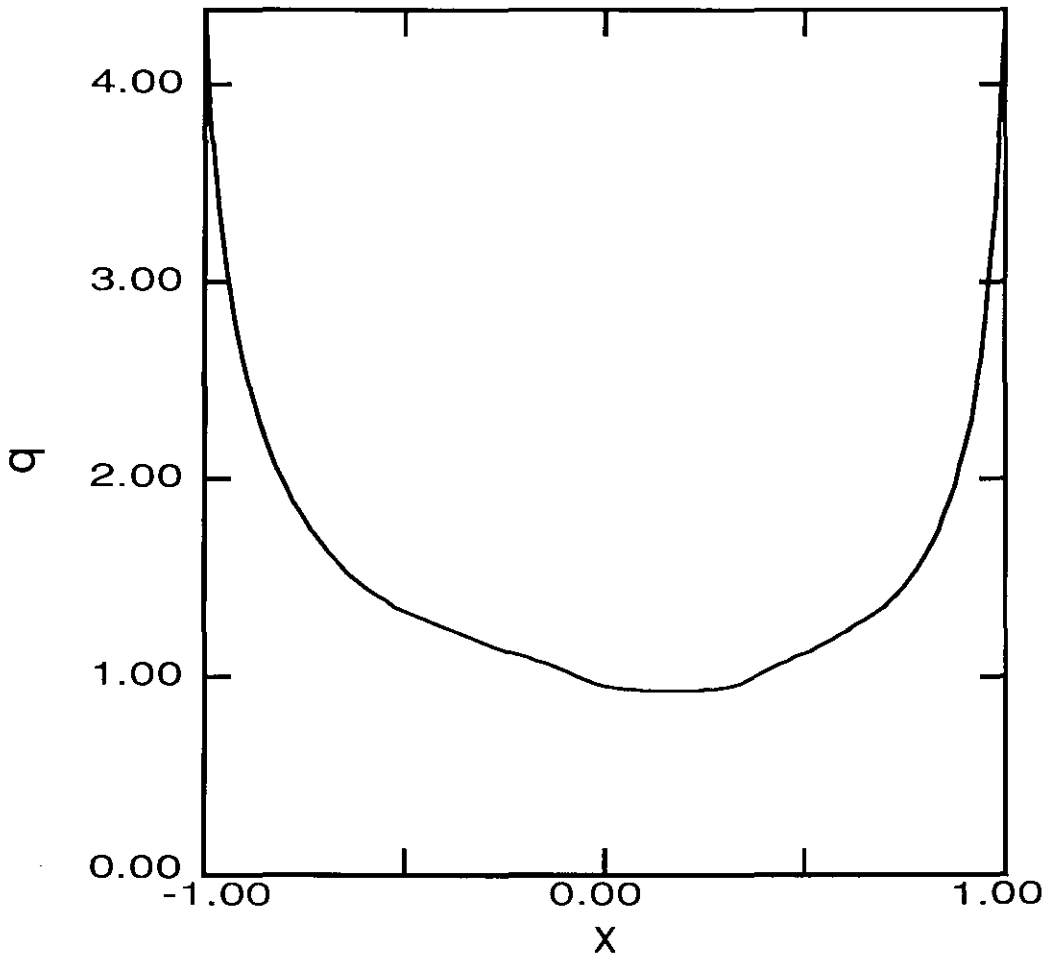

Fig. 13 The q-profile of the equilibrium of discharge #20272, t = 52.5 s.

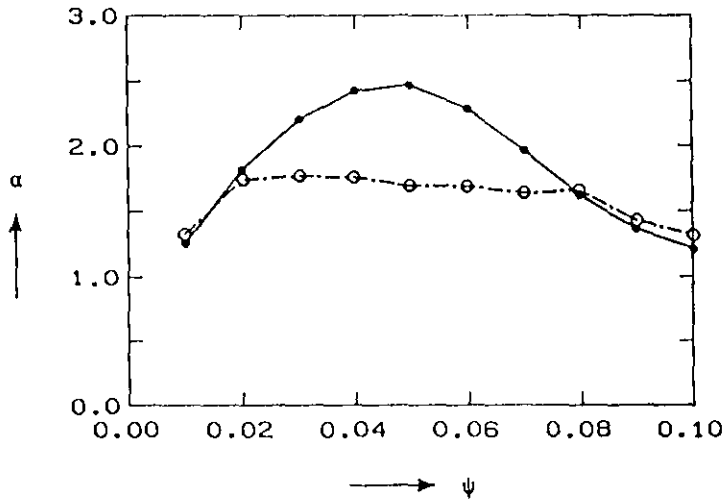

Fig. 14 The normalized pressure gradient as a function of the flux of the marginally stable equilibrium (open dots) and of the experimental equilibrium (filled dots) in the plasma center of discharge #20272.

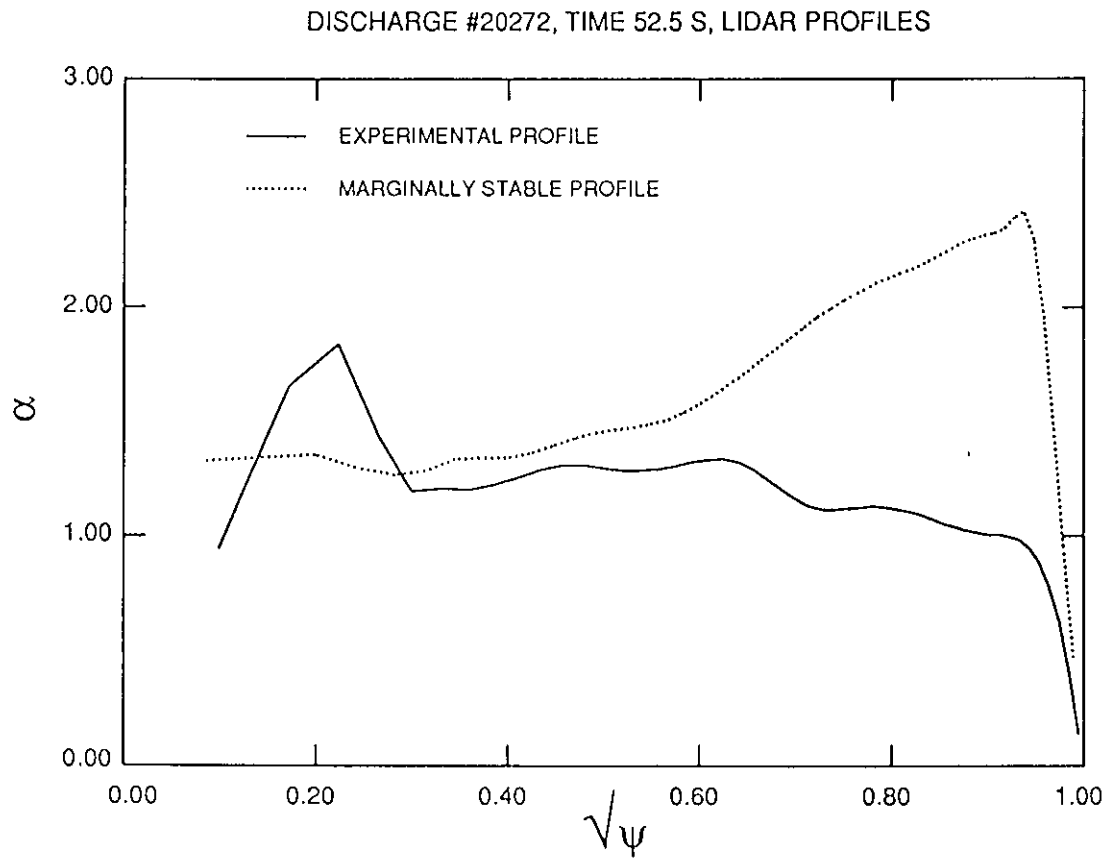

Fig. 15 A comparison of the pressure gradient profile of the reconstructed equilibrium and of the marginally stable pressure gradient profile of discharge #20272, t = 52.5 s.

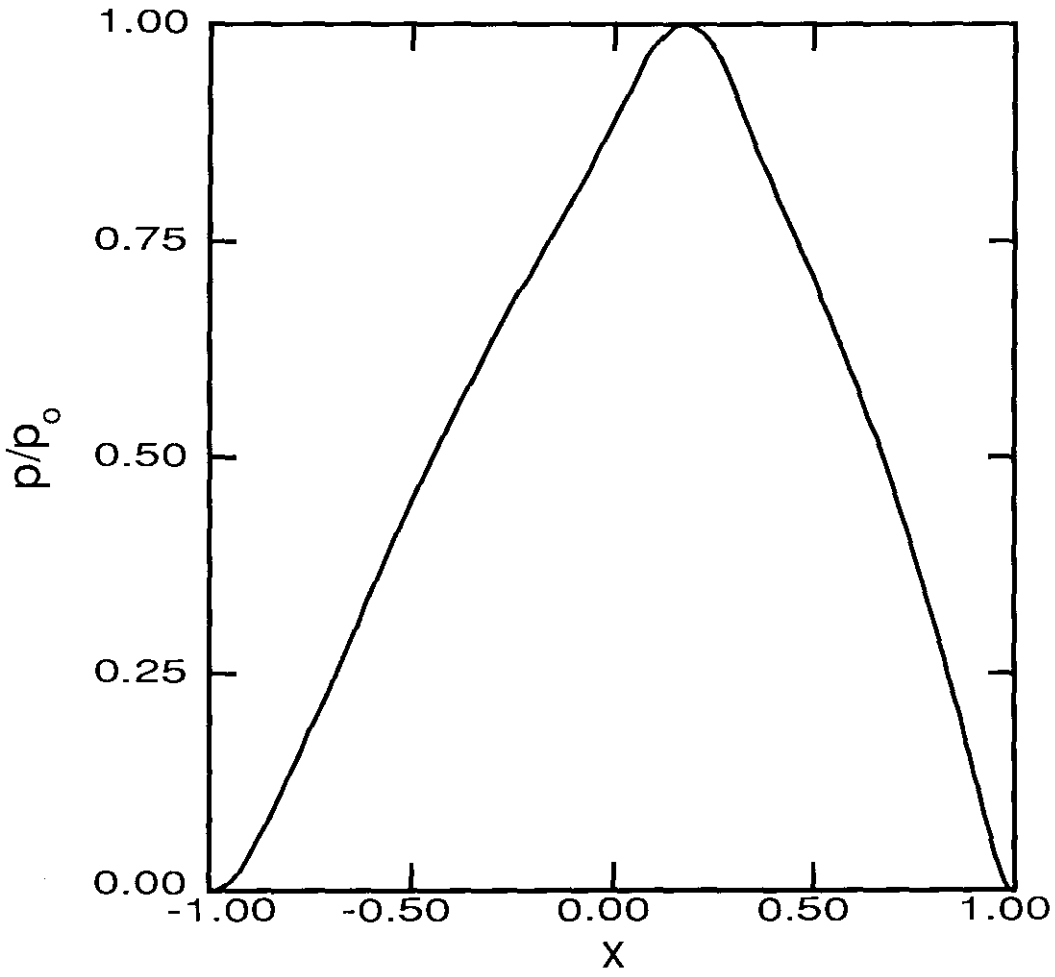

Fig. 16 The pressure profile corresponding to the marginally stable pressure gradient profile of discharge #20272.

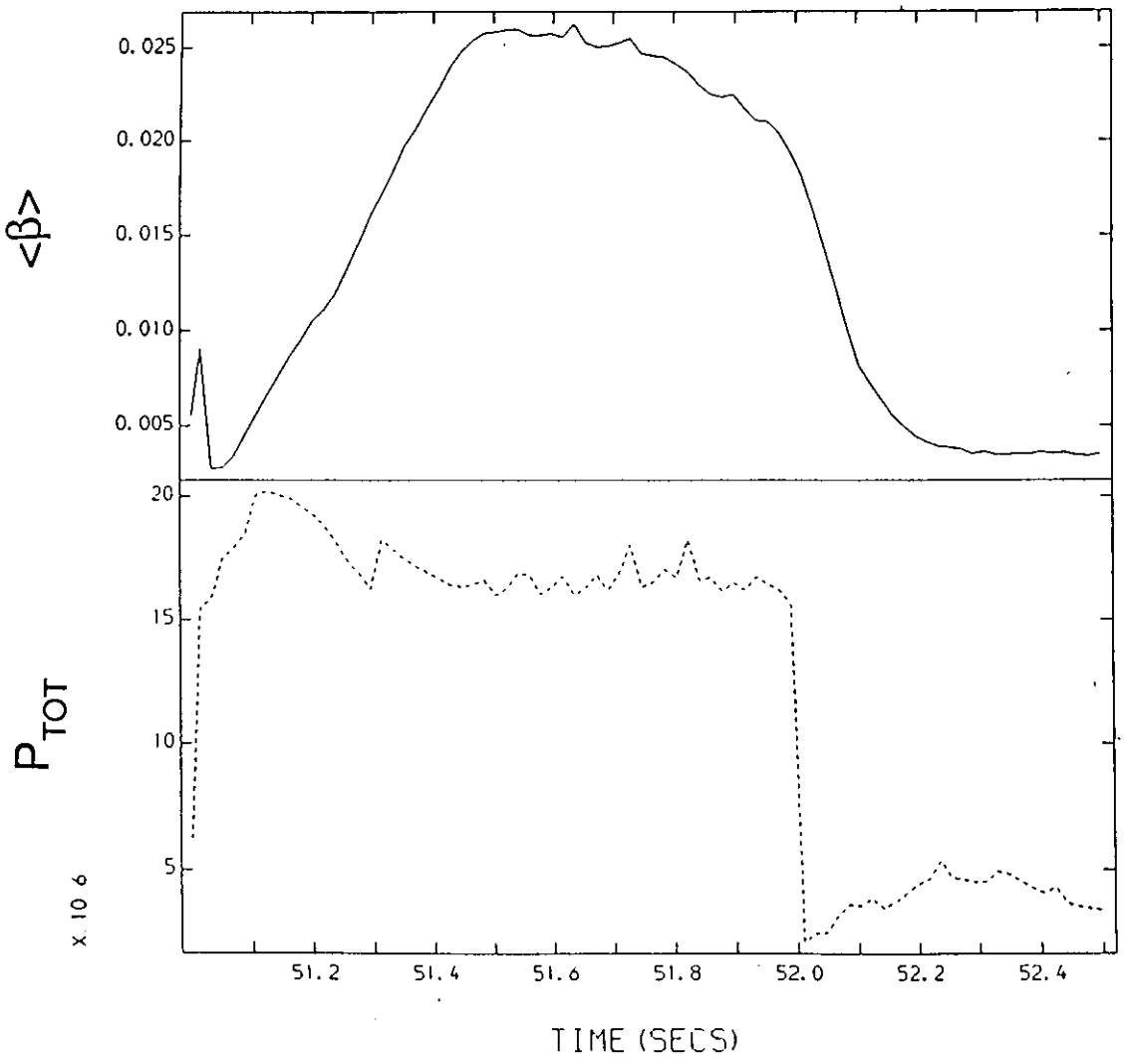

Fig. 17 The traces of the toroidal beta and the total heating power of discharge #20302.

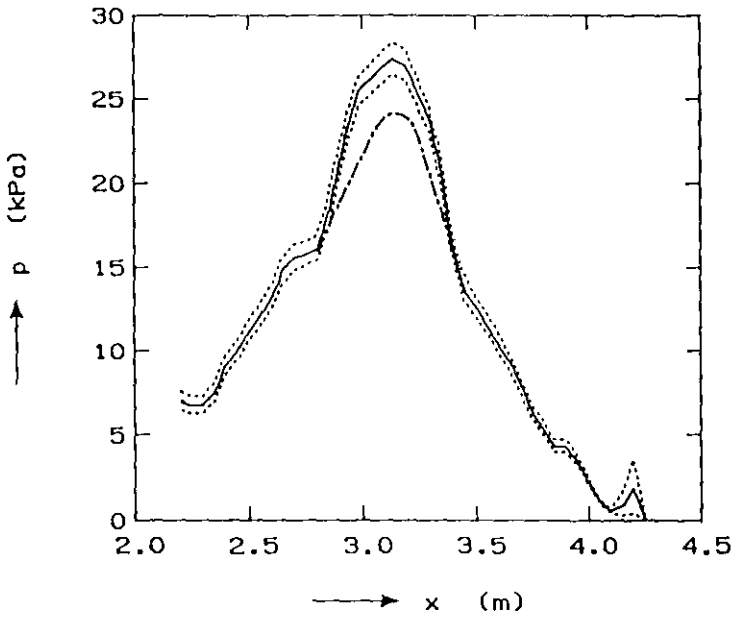

Fig. 18 The electron pressure profile obtained from the LIDAR diagnostic of discharge #20302, t = 51.5 s, with the upper and lower limits of the error bars (dashed curves). The lowest curve in the center represents the pressure profile that is marginally stable in the plasma center.

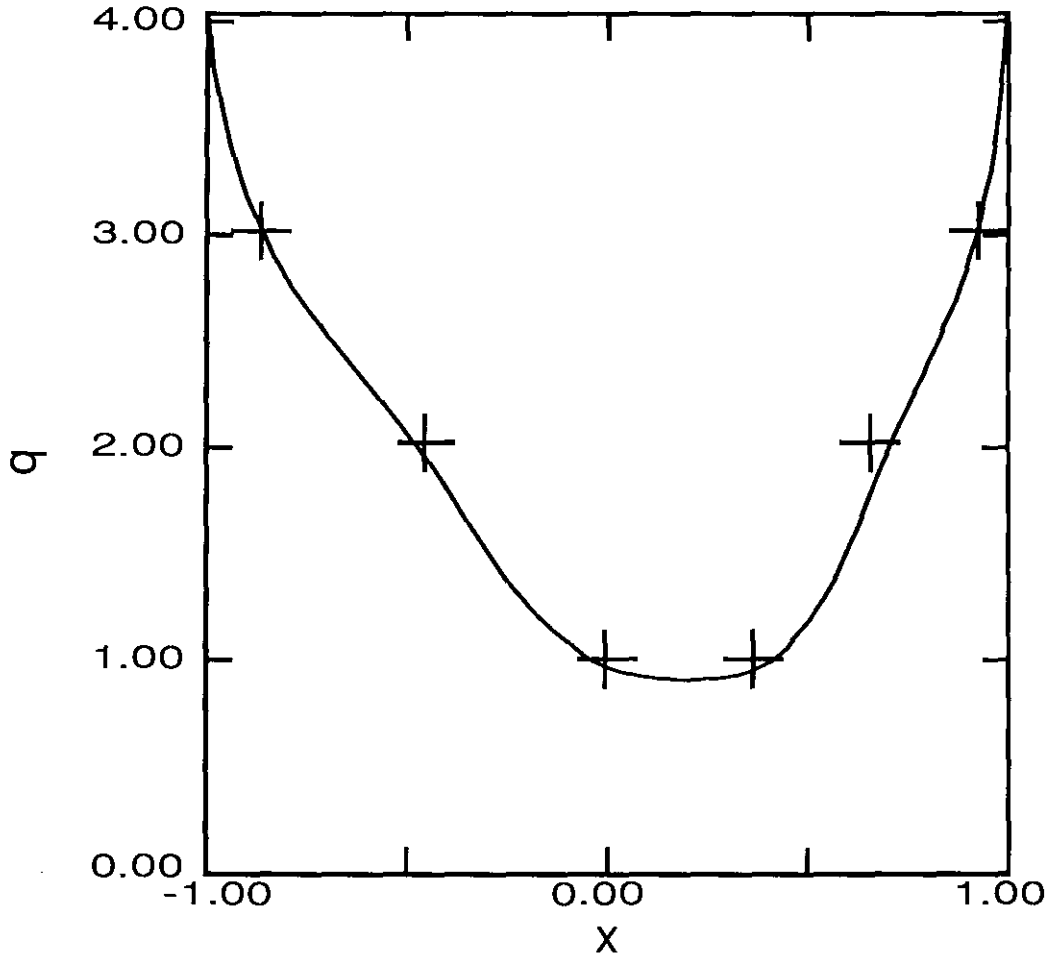

Fig. 19 The normalized q-profile of discharge #20302, t = 51.5 s. The crosses indicate the maxima of the displacement obtained from SXR data.

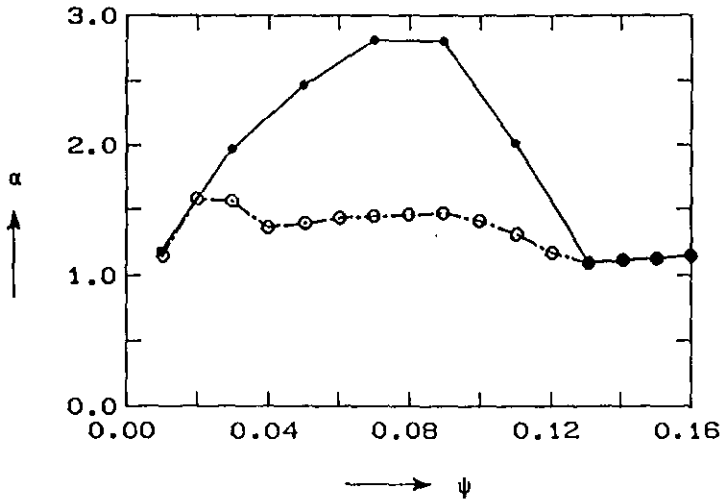

Fig. 20 The profiles of the normalized pressure gradient of the experimental equilibrium (filled dots) and of the equilibrium that is marginally stable (open dots) in the plasma center.

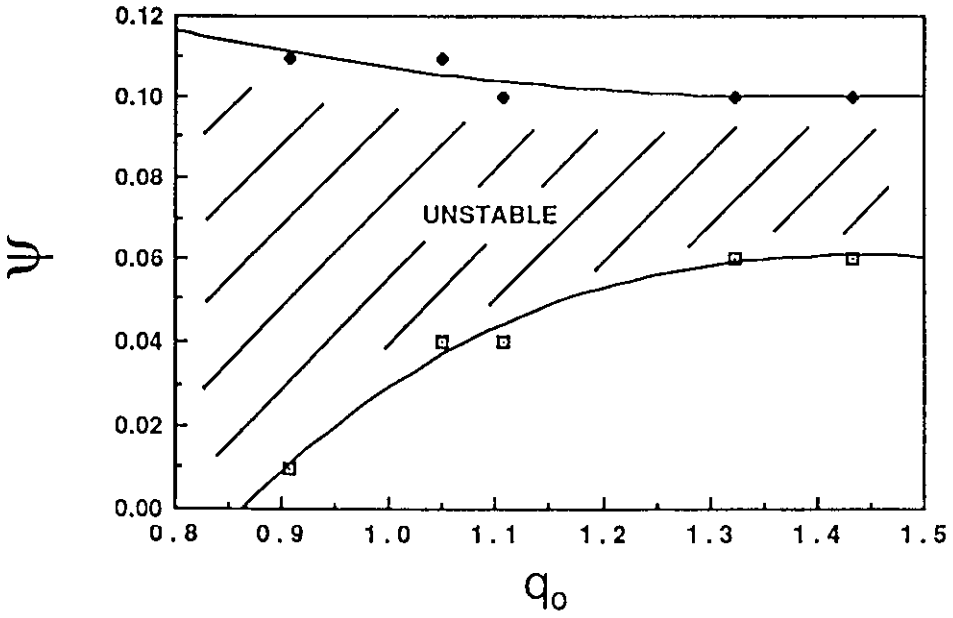

Fig. 21 The size of the ballooning unstable region as a function of q on axis.

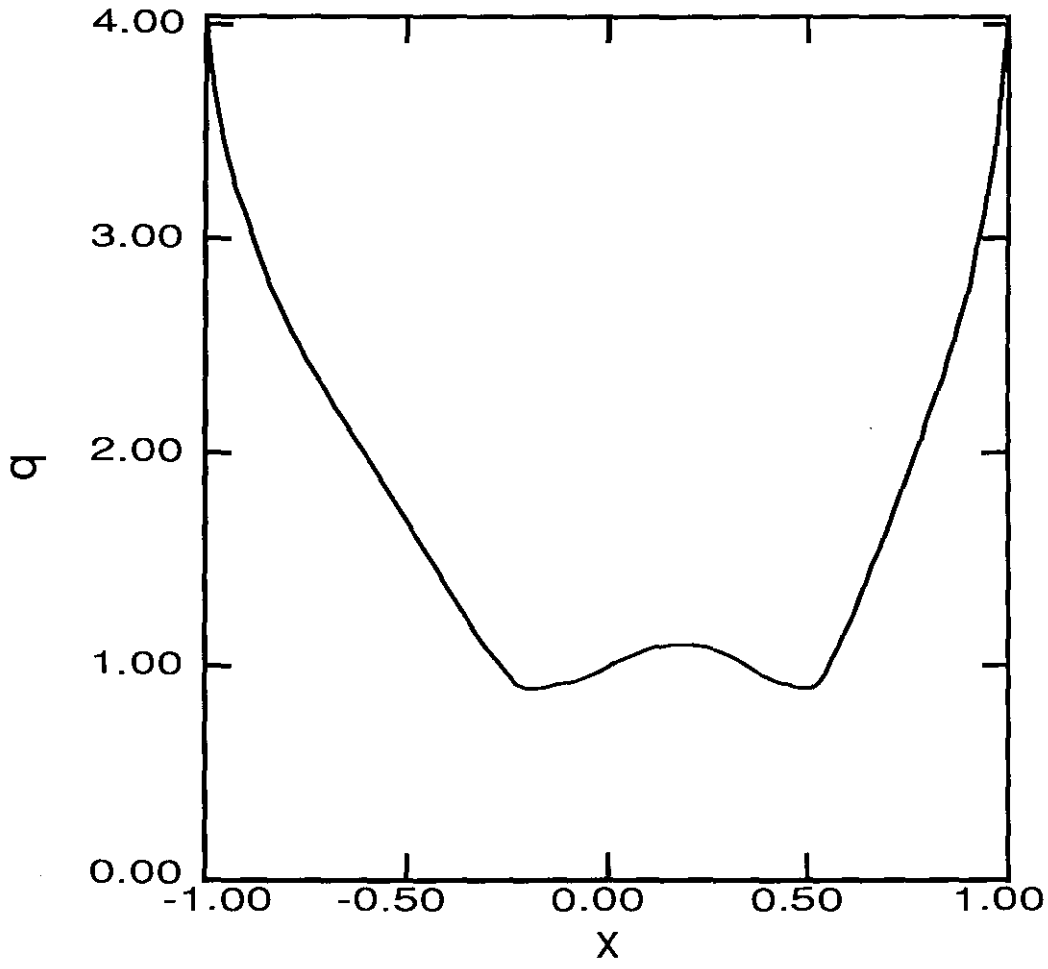

Fig. 22 The q-profile for which the equilibrium with the pressure profile of Fig. 18 is marginally stable to ballooning modes in the plasma center.

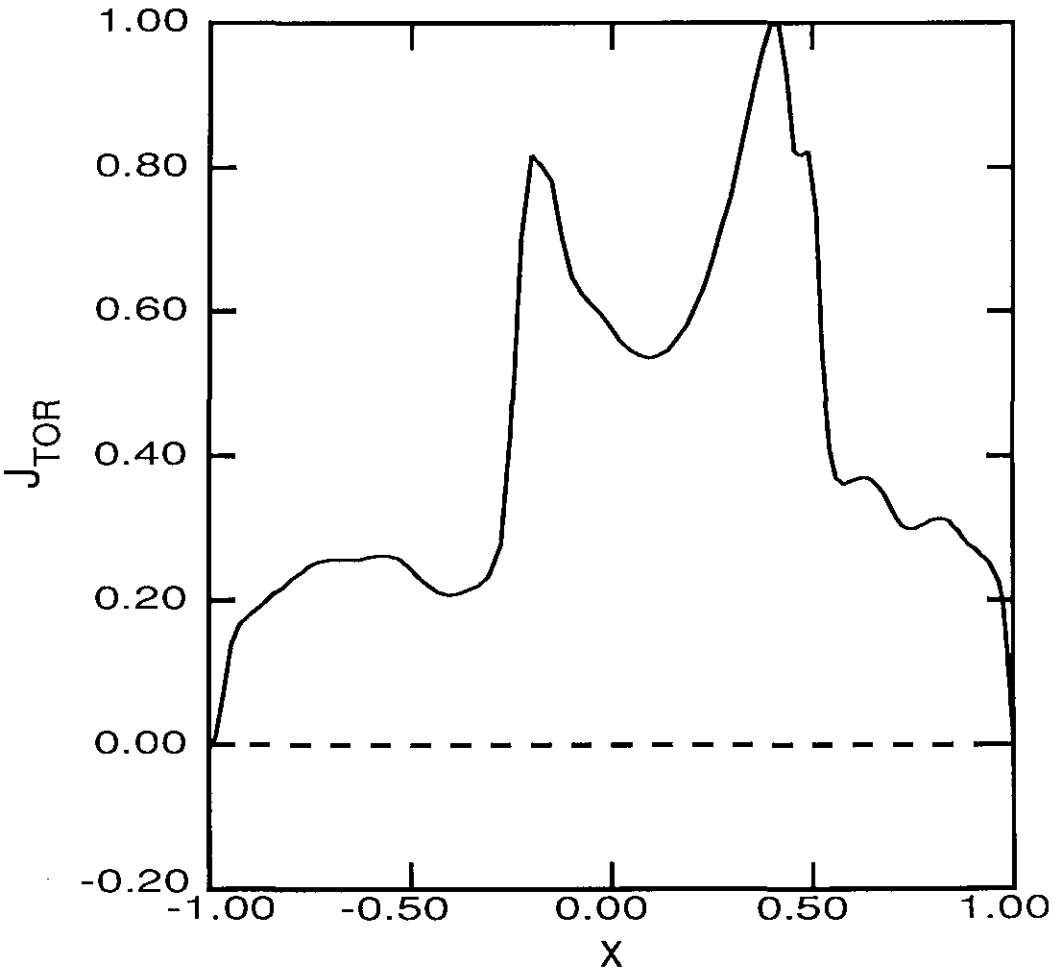

Fig. 23 The current density profile of the equilibrium with the non-monotonic q-profile of Fig. 22.

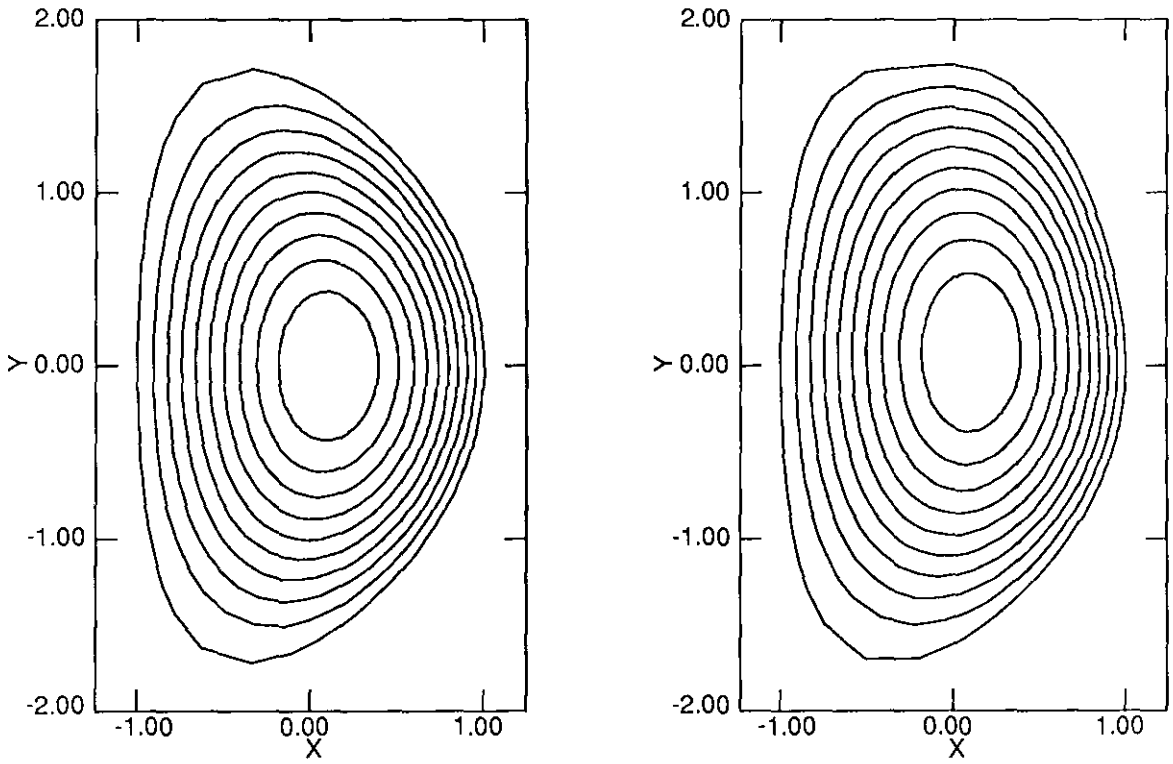

Fig. 24 The equilibrium flux surfaces of the double x-point plasma (left) and the single x-point plasma (right).

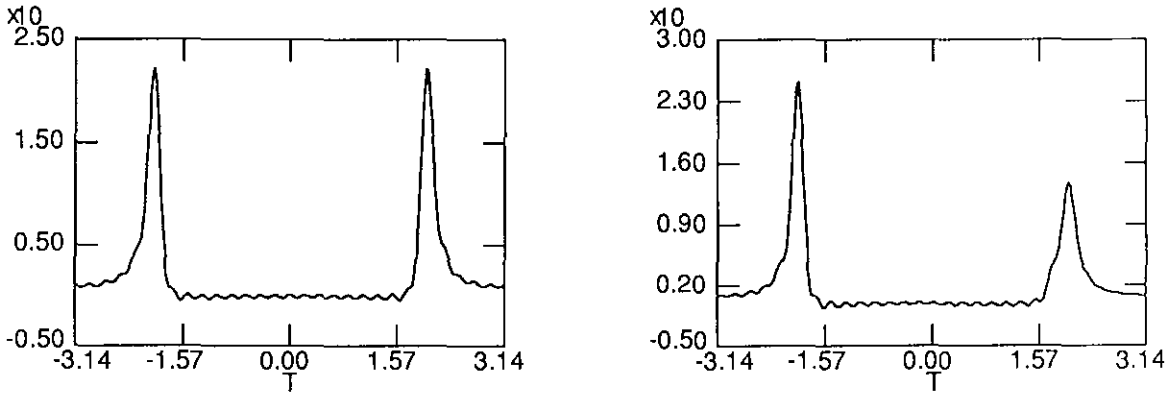

Fig. 25 The local shear as a function of the poloidal angle on the $\psi = 0.8$ surface for the two equilibria of Fig. 24 ,i.e. for the double x-point (left) and the single x-point (right)

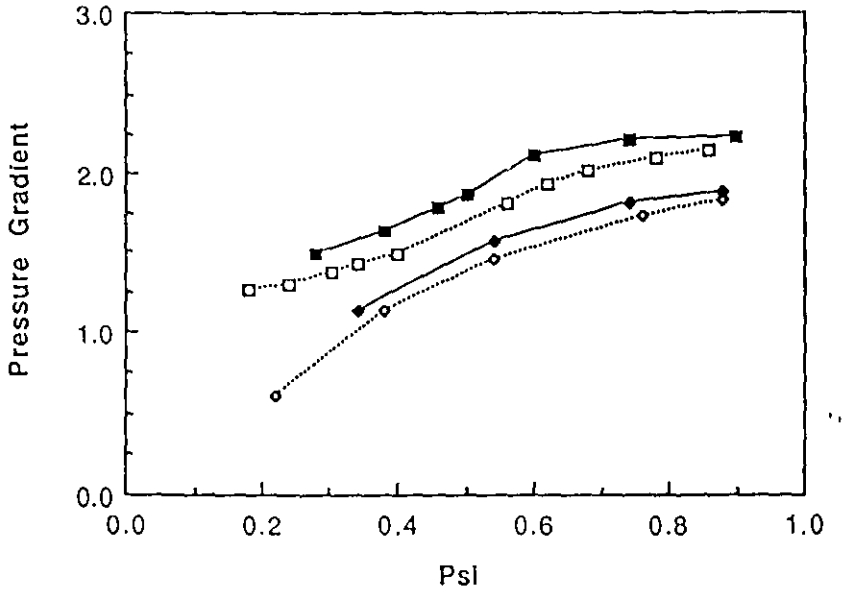

Fig. 26 Comparison of the marginally stable pressure profiles for a double and a single x-point plasma shape. The lower two curves belong to the equilibrium with a broad pressure profile (#19970), the upper two belong to the case with a peaked pressure profile (#20272). The dashed curves represent the single x-point curves, the full lines the double x-point curves.

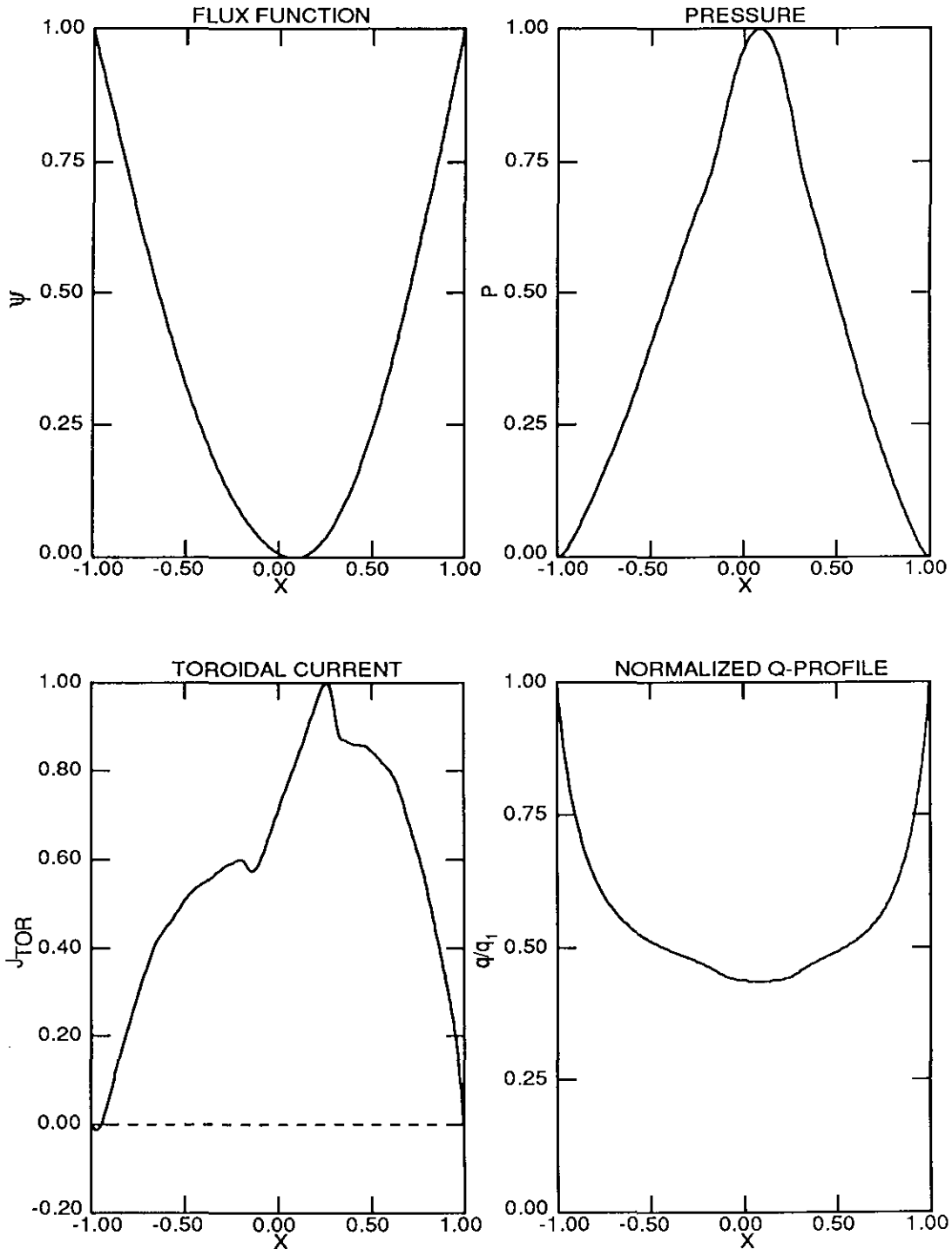

Fig. 27 The profiles of the flux, the pressure, the toroidal current and the q-profile of the high beta equilibrium of discharge #20272.

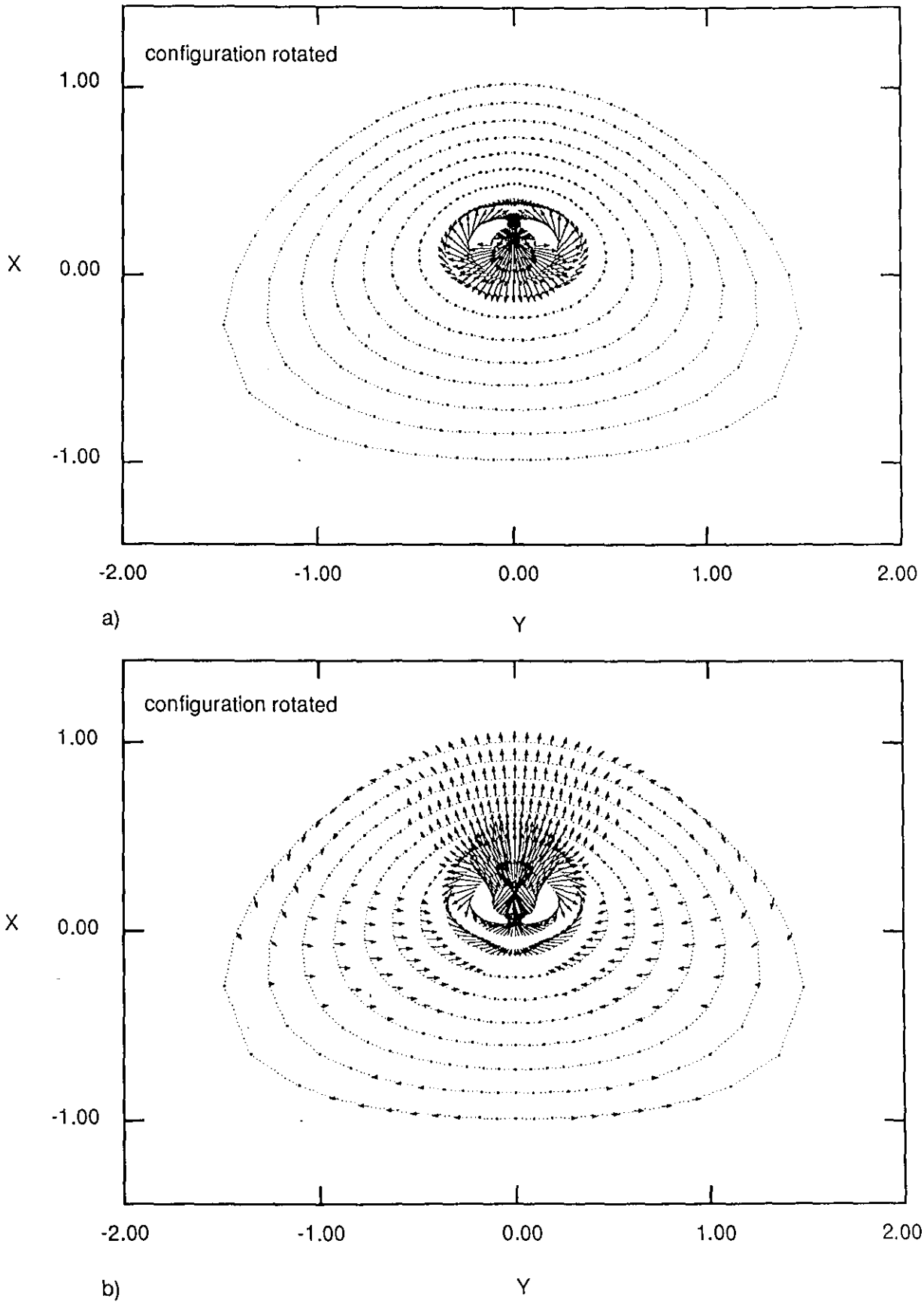

Fig. 28 The flow pattern of the mode of the high beta equilibrium of discharge #20272 at the Troyon limit. a) with the wall on the plasma. b) with the wall at infinity.

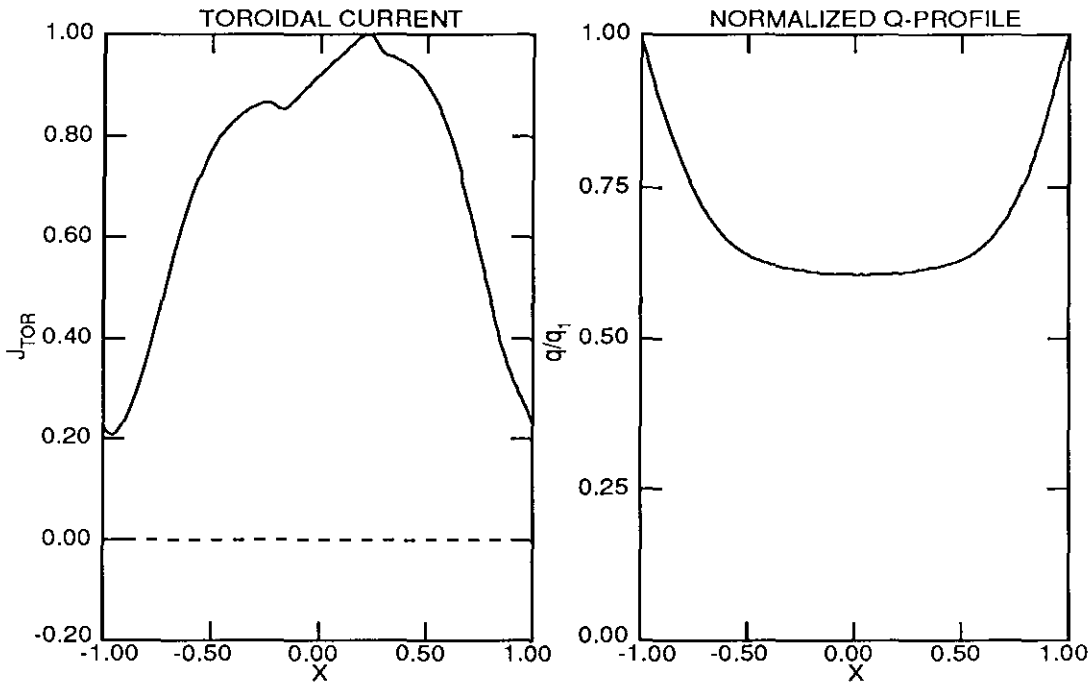

Fig. 29 The toroidal current density profile with a finite current at the edge and the resulting q-profile of the equilibrium used in the stability calculations of the peeling mode.

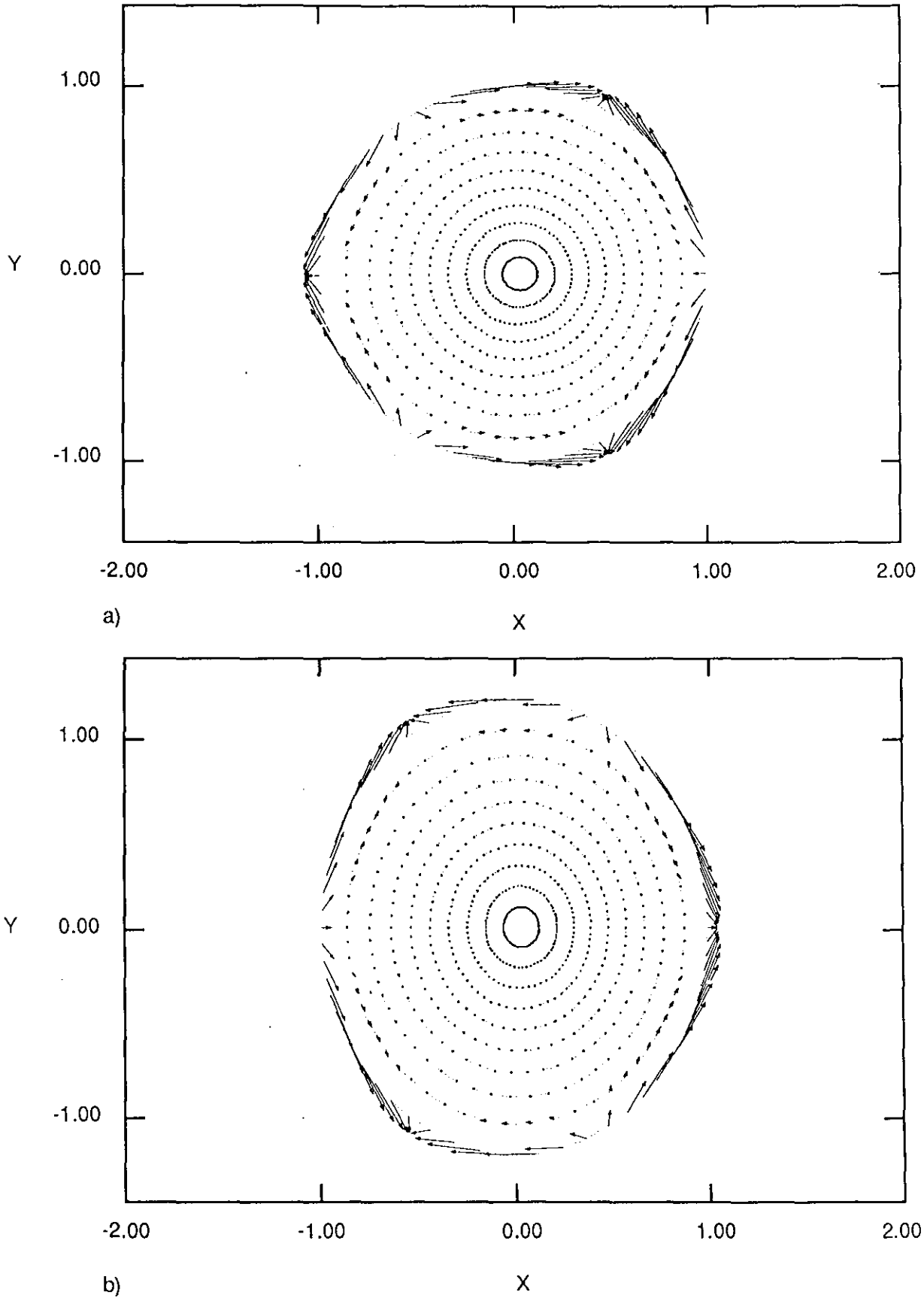

Fig. 30 The flow patterns of the peeling mode for different ellipticities. a) $\kappa = 1.0$ b) $\kappa = 1.2$